Mathematical Modelling of Nano-Electronic Systems

A Thesis

Submitted to the College of Graduate Studies and Research

in Partial Fulfillment of the Requirements

for the degree of

Doctor of Philosophy

in the

Department of Mathematics and Statistics

University of Saskatchewan

Saskatoon

By

Arash Shamloo

Permission to Use

In presenting this thesis in partial fulfillment of the requirements for a Postgraduate degree from the University of Saskatchewan, I agree that the Libraries of this University may make it freely available for inspection. I further agree that permission for copying of this thesis in any manner, in whole or in part, for scholarly purposes may be granted by the professor or professors who supervised my thesis work or, in their absence, by the Head of the Department or the Dean of the College in which my thesis work was done. It is understood that any copying or publication or use of this thesis or parts thereof for financial gain shall not be allowed without my written permission. It is also understood that due recognition shall be given to me and to the University of Saskatchewan in any scholarly use which may be made of any material in my thesis.

Requests for permission to copy or to make other use of material in this thesis in whole or part should be addressed to:

Head of the Department of Mathematics and Statistics
University of Saskatchewan,
Saskatoon, Saskatchewan, Canada
S7N 5E6

Abstract

Double-Qdots (DQDs) are attractive in light of their potential application to quantum computing and other electronic applications, e.g. as specialized sensors. We consider the electronic properties of a system consisting of two quantum dots in physical proximity, which we will refer to as the DQD. Our main goal is to derive the essential properties of the DQD from a model that is rigorous yet numerically tractable, and largely circumvents the complexities of an ab initio simulation. To this end we propose a class of novel Hamiltonians that captures the dynamics of a bi-partite quantum system, wherein the interaction is described via a convolution or a Wiener-Hopf type operator. We subsequently describe the density of states function and derive the electronic properties of the underlying system. Our analysis shows that the model captures a plethora of electronic profiles which serves as evidence for the versatility of the proposed framework for DQD channel modelling.

A massive body of mathematical physics results, dating mostly to the last half a century, give evidence to the claim that the statistical characteristic of fluctuations in the level structure of a quantum system provides essential information about its dynamic properties, e.g. in some instances these statistical parameters show whether or not the underlying classical dynamics is integrable or chaotic. Following this tradition we have conducted statistical analysis of the data generated numerically from the model at hand. In this way we have characterized the fine-scale fluctuations of the spectra for several choices of the constituents. In conclusion, we have found that the model is versatile enough to produce several statistically distinct types of level structure. In particular, the model is capable of reproducing very complex level structures, such as those of the resonant microwave cavities that have been obtained experimentally in the 1990s.

Acknowledgements

I would like to express my very great appreciation to my supervisor Prof. Artur Sowa for his valuable and constructive suggestions during my study and development of this thesis. His willingness to give his time so generously has been very much appreciated. I learned a lot from him, mathematically and non-mathematically. I thank Prof. Raj Srinivasan, the Department Head, for granting the financial support during my last year of study. I also thank my advisory committee and most specially Prof. J. Szmigielski and Prof. M. Ghezelbash.

I am greatly indebted to Prof. A. Richter and Prof. C. Rangacharyulu for generously providing experimental data.

Last but not least, I would like to express my gratitude to my friend Mehdi Rostamiforooshani for his stimulating conversations on various matters of statistics.

Arash Shamloo

Saskatoon, Summer 2014

To my mother and in memory of my father

Contents

Permission to Use i

Abstract ii

Acknowledgements iii

Contents v

Introduction 1

1 Preliminaries from Mathematics and Physics 7
- 1.1 Preliminaries from mathematics . . . 7
  - 1.1.1 Spectral theorem . . . 7
  - 1.1.2 Integral operators . . . 10
- 1.2 Preliminaries from Quantum Mechanics . . . 12
  - 1.2.1 General background . . . 12
  - 1.2.2 Axioms of quantum mechanics . . . 13
  - 1.2.3 Quantum composite systems and tensor product . . . 15
  - 1.2.4 The physics notation . . . 17
  - 1.2.5 Quantum Harmonic Oscillator . . . 18
- 1.3 Quantum mechanics in electronics . . . 23
  - 1.3.1 The quantum dot . . . 23
  - 1.3.2 The quantum-effect devices . . . 28
  - 1.3.3 Electron transport . . . 32
- 1.4 The Jaynes-Cummings model. . . . 36

2 A Numerically Efficient Approach to the Modelling of Double-Quantum Dot Channels 41
- 2.1 Introduction . . . 41
- 2.2 Constructing the composite system Hamiltonian . . . 44
- 2.3 Examining the special case . . . 46
- 2.4 Modelling a double-Qdot channel . . . 49
- 2.5 Numerical Experiments . . . 53
- 2.6 Qualitative comparison to the experimental data . . . 57
- 2.7 A discussion of numerical efficiency . . . 58
- 2.8 Chapter conclusion . . . 61

3 Fine Scale Spectral Analysis 62
- 3.1 Introduction . . . 62
- 3.2 A statistical methodology for the analysis of Hamiltonian dynamics . . . 65

3.3 Statistical analysis of the double quantum dot model 68
3.4 A comparison with real quantum data 74

A Some statistical tools **79**
A.1 Quantile-Quantile plot (Q-Q plot) 79
A.2 The Kolmogorov-Smirnov test 81

B MATLAB Codes **85**
B.0.1 The numerical algorithms corresponding to Chapter 2 85
B.0.2 The numerical algorithms corresponding to Chapter 3 92

References **99**

Introduction

Semiconductor quantum dots (QDs) are man-made nano-size structures typically comprised of 10^3 – 10^9 atoms with equivalent number of electrons as well as tractable size and shape [46]. Electrons are confined in all three dimensions in these nano-structures. Therefore, their energies are quantized. Because of that they are called artificial atoms [2]. In particular, the idea of using double quantum dots (DQD) in quantum computing devices has attracted much interest and led to the development of experimental techniques, see [74, 29]. One of the remarkable examples is a double-Qdot comprising two *single-electron* quantum dots, see [61, 21]. Since these double-Qdots provide a means for controlling the charge qubits and spin qubits via gate potentials— the latter ones implementing a spin-swap which is a fundamental quantum computing operation, [48]—they may well become the enabling hardware components of a quantum computer. Moreover, the DQDs have been used effectively to substitute for the traditional piezoelectric sensors, [45].

In this regard the topic attracts quit a bit of attention, and it is necessary to develop good models for the electronic structure of DQDs systems. The main focus of my work has been to try and improve upon the current state of the art in the area of nano-circuit simulation with particular focus on the existing example of DQDs. I have attempted to find an elemental, mathematically rigorous, and physically correct model for the DQD. I have subsequently tested my hypothesized model by means of applying it to drive predictions about the behaviour of physical systems. Based on numerical experimentation, I find that the proposed approach captures the essential electronic features of the DQD. I also believe that the proposed simulation algorithms may be scaled and extended via future research work to assist in realistic large scale simulation and modelling work for applications such as nano-circuit analysis and quality control.

I have strived to improve upon the pre-existing approaches to quantum dot modelling, such as:

- ***The quantum master equation (QME)*** The dynamics of open quantum systems have been studied extensively in the field of quantum optics, [30]. The main goal in this approach is to describe the time evolution of an open system via the quantum master equation that describes non-unitary behaviour (irreversible dynamics of a quantum systems coupled to two contacts). Recently, it has been used to study electron tunnelling through DQDs, [39, 49, 60].

- ***Scattering Matrix (SM)*** Scattering matrix is limited to the elastic resistors that their resistance determined by the channel, but the corresponding heat is entirely dissipated in the contacts. This method has been used to for predicting current-voltage characteristics of a quantum system connected to two metal contacts,[14].

- ***The non-equilibrium Green's function (NEGF)*** In order to study characteristics of electron-electron interaction inside the QDs, researchers have applied many body perturbation theory (MBPT), see [69, 81]. Of note is the Hartree-Fock approximation method. But it is well established that this method overestimates the interaction potential and there are various approaches for estimating this reduction. One of these methods is density functional theory (DFT), [18]. Although this theory is successful in describing the correction for equilibrium problems it is not too useful in explaining the non-equilibrium phenomena such as current flow, [18]. The non-equilibrium Green's function theory has been developed to correct this failure. Particularly, in [48] the authors assessed the validity of the equation of motion approach to the NEGF formalism specifically for a double-Qdot coupled with two contacts. The model takes into account both intra- and intro-dot Coulomb interactions. In general, the equation of motion NEGF formalism provides a qualitative description of transport phenomena that occur in strongly correlated systems, such as the Coulomb blockade effect. The authors study the effect of different approximate closures to the equation of motion NEGF formalism on steady state properties

within an extended Hubbard model (also known as the double Anderson model). For comparison in [74] the authors consider a NEGF model based on a Hubbard-type Hamiltonian, which accounts for tunnelling type electron transfer between the two Qdots as well as the isolator-type electrostatic Coulomb interaction between them. The effect of contacts is also modelled via a tunnelling electron transport. The (NEGF) can treat both elastic and inelastic processes, so this is one of the advantages of (NEGF) approach to (SM) approach, [39].

Both of the models of a double-quantum dot, the *ab initio* one, say, the Hartree-Fock approximation and the NEGF theory require intensive computation. In Chapter 2 I undertake to consider a novel model for a DQD which enables some scalability of computational complexity. The model based on a Hamiltonian for a bipartite quantum system, wherein the subsystem Hamiltonians are given *a priori*, and the interaction term is constructed with the use of a convolution or a Wiener-Hopf type operator. My motivation to focus on this type of interaction resulted from a principle of succinctness, the "Occam's razor", which states that among competing hypotheses, the one with the fewest assumptions should be selected. The model must, first, incorporate each single dots dynamics and, second, it must account for the Qdot-Qdot interaction. We emphasize that the interaction is modelled at a rather general level to avoid the complexity trap that would be inevitable in an *ab initio* approach. The type of construction being proposed is perhaps somewhat reminiscent of the classical Jaynes-Cummings model, [40, 70], frequently evoked in Quantum Optics. However, in stark contrast to the Jaynes-Cummings Hamiltonian our model incorporates a high-dimensional parameter (the kernel function) which makes it possible to adjust the model to the specific classification of any particular physical system of the given type.

One of the main goals of Chapter 2 is to examine the cumulative density of states function, $N(E)$, arising from the proposed Hamiltonian. Extensive numerical simulations have been conducted to examine the dependence of $N(E)$ on the choice of the parameters K, the kernel, whose role is to capture qualitatively the inter-Qdot interaction, and λ, the interaction strength moderator. In section 2.5, we demonstrate numerically that the

kernel function strongly affects the characteristics of $N(E)$. One of my main results is depicted in Figure (2.7) which evidences the model's versatility and predicts at least three different electronic categories. In Section 2.6 a qualitative comparison of these predictions to the known experimental data is given. These data resulted from an experiment conducted over single electron transport through a DQD. In Section 2.7 I discuss a range of issues relating to the numerical efficiency of the model. Material presented in this Chapter has appeared in print, [68].

A set of mathematical tools has been developed in the previous decades to model and understand the fundamental characteristics of atomic nuclei. It remains to be seen if the fundamental characterisation of nano-systems is similar or rather different in some fundamental way. In Chapter 3 I embark on a project to see if the known methodology, including the methods for constructing quantum Hamiltonians, may be used to model the fundamental behaviour of nano-systems. In particular, I ask if the spectral properties of objects such as quantum dots are similar or different from those of atomic nuclei. I have applied the apparatus of statistical analysis of spectra, as first developed by the theorists of semiclassical physics, to see whether or not any definitive statements could be made on the comparison between the nano and the nuclear. The main idea that led to the introduction of statistical methods, specifically the *Random Matrix Theory* (RMT), was the notion of complexity that nowadays is referred to as *chaos* which is related to the large number of degrees of freedom involved in a many-body problem. Since nano-systems are many-body systems it is reasonable to expect that the level statistics of such systems are described by the RMT or a similar framework.

Researchers have employed statistical methods to the spectrum of atomic systems in order to determine whether the system is integrable or chaotic. Distinguishing between integrable and chaotic systems requires considering the *fluctuation* of energy levels; that is, how the energy levels are distributed around the average density of states. Since energy levels corresponding to different systems or different regions of energy levels of the same system may have different *average* density, one must unify the average density before comparing fluctuations. To this end one must renormalize (*unfold*) the levels of

energy.

The simplest quantity that describes the level fluctuations is the nearest neighbourhood spacing distribution (NNSD) $p(s)$ where $p(s)ds$ is the probability of finding two adjacent unfolded energy levels in $[s, s+ds]$. For the quantum systems whose underlying classical system is integrable, Berry and Tabor in [7] show that $p(s)$ is universal and is a Poisson distribution. It was conjectured by Bohigas, Giannoni and Schmit [9], that the NNSD of the spectra of a quantum system whose classical analogue is fully chaotic can be predicted by the Gaussian Orthogonal Ensemble (GOE). There is numerical evidence as well as analytical arguments supporting this conjecture; see [6]. The best approximation to the NNSD for the GOE is given by the *Wigner distribution* 3.2.3, [80, 62]. Brody generalized the Wigner distribution in order to study *mixed* (partialy chaotic) systems to a distribution with a parameter b which is called the repulsion parameter, [12].

As mentioned above, in order to determine the NNSD, it is necessary to unfold the original spectra. To this end, In section 3.2 the methodology of unfolding is discussed and equation 3.2.2 is taken into account. In section 3.3 the statistical analysis of the DQD model is studied in detail. The method of moment estimate is applied to find the best repulsion parameter in order to approximate NNSDs by the Brody-type distributions. Accordingly, the most important outcomes of this section are illustrated in figures 3.3 and 3.4 which show the NNSDs as well as their approximations by the appropriate Brody distributions. Afterwards, the two methods of quantile-quantile plot (A.1) and Kolmogorov-Smirnov (A.2) are employed to confirm the accuracy of the introduced approximations. The author has not been able to find an actual experimental spectrum data for an interacting DQD. Instead, however, in section 3.4 a comparison with experimental data from a real quantum system, courtesy of A. Richter and C. Rangacharyulu, is made. These data were generated by means of an experiment on a two-dimensional superconducting microwave resonator shaped like a quarter of a stadium billiard, [31]. I refer to these data as the Richter data throughout the thesis. It is demonstrated that a specific type of spectrum of the model at hand and actual data have the same distribution, even though they come from an application of seemingly non-congrouent approaches. Further-

more, my purely quantum model captures approximately the same repulsion parameter as the experimental data interpreted via the semiclassical theoretical apparatus.

Chapter 1

Preliminaries from Mathematics and Physics

In order to introduce the novel model for a quantum composite system and derive the essential electronic properties of a double quantum dot from the model we require some background knowledge from operator theory as well as quantum mechanics and semi-conductor theory. Accordingly, these subjects are introduced in this chapter.

1.1 Preliminaries from mathematics

1.1.1 Spectral theorem

An operator is bounded if its norm is a non-negative real number. According to the Hellinger-Toeplitz theorem [64] any symmetric operator defined on the entire Hilbert space is bounded. To put this fact the other way around, an unbounded self-adjoint operator can not be defined on the entire Hilbert space. It is defined on a dense subset, *the Domain*, of the relevant Hilbert space. Although we know most of the operators in quantum mechanics are unbounded, in this preliminary section our emphasise is on bounded operators. Most systems stay close to the ground state. In other words, the electrons will hardly ever go very high on the energy ladder. So the shape of the ladder very high up really does not matter in most considerations. So, for applications, such as to electronic modelling, the finite dimensional approximation is good enough. Sometimes we still use infinite-dimensional operators, but mostly when it is more convenient to do so, e.g. it would be clumsy not to consider the partition function based on all system levels in the Statistical Physics.

Let A be a bounded operator on a Hilbert space $\mathcal{H}$.

Definition 1.1.1. The resolvent set $\rho(A)$ of A consists of all complex numbers λ for which $\mathcal{R}(\lambda; A) = (A - \lambda I)^{-1}$ is a bounded operator (with domain $\mathcal{H}$). Thee *spectrum* $\sigma(A)$ of A consists of the complement of $\rho(A)$ in $\mathbb{C}$.
The operator $\mathcal{R}(\lambda; A) = (A - \lambda I)^{-1}$ if bounded is called the *resolvent* of A.
Let $\lambda \in \sigma(A)$. Then there are three possibilities [28]:

1. $\mathcal{R}(\lambda; A)$ exists and is unbounded but its range is dense in $\mathcal{H}$. We say that λ belongs to the *continuous* spectrum of A, $\sigma_c(A)$.

2. $\mathcal{R}(\lambda; A)$ exists and is bounded and its domain is not dense in $\mathcal{H}$. We say that λ belongs to the *residual* spectrum of A, $\sigma_r(A)$.

3. $A - \lambda I$ is not invertible. We say that λ is an *eigenvalue* or belongs to the *discrete* spectrum of A, $\lambda \in \sigma_d(A)$.

Theorem 1.1.1. *If operator A on Hilbert space $\mathcal{H}$ is self-adjoint, then $\sigma(A) \subseteq \mathbb{R}$. And*

$$\sigma(A) = \sigma_c(A) \cup \sigma_d(A).$$

For a proof see [28].

Example 1. *Spectrum of operator $P = \frac{1}{\iota}\frac{d}{dx}$ on $L^2(\mathbb{R})$, the operator of* momentum, *is $\mathbb{R}$. Or further $\sigma(P) = \sigma_c(P) = \mathbb{R}$.*

See [67].

Definition 1.1.2. Two operators A and B on a Hilbert space are called unitary equivalent if there exist a unitary operator U,$U^*U = UU^* = I$, such that $A = U^*BU$.

Theorem 1.1.2. *If operators A and B are unitary equivalent then $\sigma(A) = \sigma(B)$.*

see [67].
Next, I express the *spectral theorem* in its rather general form adopted from [64].

Theorem 1.1.3. (Spectral theorem—multiplication operator form) *Let A be a bounded self-adjoint operator on a separable Hilbert space $\mathcal{H}$. Then, there exists measures $\{\mu_n\}_{n=1}^{N}$ $(N = 1, 2, \cdots, \infty)$ on $\sigma(A)$ and a unitary operator*

$$U : \mathcal{H} \longrightarrow \bigoplus_{n=1}^{N} L^2(\mathbb{R}, d\mu_n)$$

so that

$$(UAU^{-1}\psi)_n(\lambda) = \lambda\psi_n(\lambda)$$

where $\psi(\lambda) = (\psi_1(\lambda), \cdots, \psi_N(\lambda))$.

For a proof see [64].

Remark 1.1.3. If $\mathcal{H} = L^2(\mathbb{R}, dx)$,

$$(UAU^{-1}\psi)_n(\lambda) = (A\psi)(\lambda) = \lambda\psi(\lambda)$$

where $U : L^2(R) \longrightarrow L^2(R)$.

Definition 1.1.4. Let $u : \mathbb{R}^2 \longrightarrow \mathbb{C}$ be a continuous function and the operator M on $L^2(\mathbb{R})$ acting by the rule

$$M_u(\psi)(x) = u(x)\psi(x) \quad \forall \psi(x) \in L^2(\mathbb{R}).$$

M_u is called the *operator of multiplication* by the continuous function u. In the special case if $u = x$ for an independent variable x,

$$M_x(\psi)(x) = x\psi(x) \quad \forall \psi(x) \in L^2(\mathbb{R})$$

or, following quantum-mechanics terminology, *the coordinate operator*.

Example 2. *The spectrum of the operator of multiplication, M, on $L^2(\mathbb{R})$ is*

$$\sigma(M) = \sigma_c(M) = \mathbb{R}.$$

See [67].

Remark 1.1.5. Since $\forall\lambda \in \mathbb{R},\ (x-\lambda)\delta(x-\lambda) = 0$ therefore $\delta(x-\lambda)$ is a solution of $Mu = \lambda u$, but $\delta(x-\lambda) \notin L^2(\mathbb{R})$

Example 3. *Let* $\Delta = -\frac{d^2}{dx^2}$ *on* $L^2(\mathbb{R})$. *Then*

$$\sigma(M) = \sigma_c(M) = [0, \infty).$$

Proof. According to theorem 1.1 the spectrum of the momentum operator $P = \frac{1}{\iota}\frac{d}{dx}$ *is* $\sigma(M) = \sigma_c(M) = \mathbb{R}$. *and by remark 1.1 functions*

$$e(x,\lambda) = \frac{e^{\iota\lambda x}}{\sqrt{2\pi}} \quad \lambda \in \mathbb{R}$$

are the generalized eigenvectors of P. On the other hand $P^2 = \Delta$. *Therefore* $e(x,\lambda)$ *is a generalized eigenfunction of operator* Δ *for eigenvalues* $\mu = \lambda^2$ *and* $e(x,\lambda) = \frac{1}{\sqrt{2\pi}}e^{\pm\sqrt{\mu}x}$. *Since* $\mu = \lambda^2$ *and* $\lambda \in \mathbb{R}$, *then*

$$\sigma(M) = \sigma_c(M) = [0, \infty).$$

In conclusion,

$$\{\frac{1}{\sqrt{2\pi}}e^{+\sqrt{\mu}x}, \frac{1}{\sqrt{2\pi}}e^{-\sqrt{\mu}x}\}_{\mu\in[0,\infty)}$$

is the set of eigenfunction of the operator Δ. Another conclusion of above theorem is that spectrum of the Schrödinger operator of a free particle is continuous.

1.1.2 Integral operators

Let $D = (a,b)$ be a finite or infinite interval in $\mathbb{R}$ and $K(x,y)$ a function on $(a,b)\times(a,b)$. The integral operator on $L^2(D)$ is the formal expression

$$(\mathbb{K}f)(x) = \int_D K(x,y)f(y)dy, \quad x \in D.$$

$K(x,y)$ is called the kernel of the integral operator $\mathbb{K}$.

Theorem 1.1.4. *Let* $\mathbb{K}$ *be an integral operator on* $L^2(D)$. *Then the kernel* $K^*(x,y)$ *of the adjoint operator* $\mathbb{K}^*$ *is given by* $K^*(x,y) = \overline{K(y,x)}$. *And for a self-adjoint integral operator we have* $\mathbb{K} = \mathbb{K}^* \Leftrightarrow K(x,y) = \overline{K(y,x)}$.

Examples

- *The Fourier transform* Let $f(x) \in L^1(\mathbb{R})$ then the Fourier transform of $f(x)$ is

$$(\mathbb{F}f)(\lambda) = \frac{1}{\sqrt{2\pi}} \int_{-\infty}^{\infty} e^{-\iota\lambda x} f(x) dx$$

and also denoted by $\hat{f}(\lambda)$. The adjoint of the Fourier transform is

$$(\mathbb{F}^* f)(x) = \frac{1}{\sqrt{2\pi}} \int_{\infty}^{\infty} e^{\iota\lambda x} f(\lambda) d\lambda$$

which is called the inverse Fourier transform and also denoted by $\check{f}(x)$.

Theorem 1.1.5. *The Fourier transform is a unitary operator on* $L^2(\mathbb{R})$.

See [67].

Remark 1.1.6. Let $f, f' \in L^1(\mathbb{R})$ then using integration by parts

$$\hat{f}'(\lambda) = \iota\lambda \hat{f}(\lambda)$$

Consequently, one can infer

$$F\left(\frac{1}{\iota}\frac{d}{dx}\right)F^{-1} = \lambda.$$

It means the operators of differentiation and multiplication by λ are unitarily equivalent. The quantum mechanical interpretation of this relation is: The coordinate and the momentum representations are equivalent.

Definition 1.1.7. If f and g belong to the $L^1(\mathbb{R})$, the *convolution* $f * g$ of these functions is defined as

$$(f * g)(x) = \frac{1}{\sqrt{2\pi}} \int_{-\infty}^{\infty} f(s) g(x - s) ds$$

The convolution has following properties:

1. $(f * g)(x) = (g * f)(x)$
2. $f * (g_1 + g_2) = f * g_1 + f * g_2$

3. $f * (g_1 * g_2) = (f * g_1) * g_2$

4. $\widehat{f * g} = \hat{f}.\hat{g}$

For proofs See [33].

- Let $\mathbb{K} = M_u$ (multiplication operator) for this operator the kernel is

$$K(x, y) = u(x)\delta(x - y).$$

See [33].

1.2 Preliminaries from Quantum Mechanics[1]

1.2.1 General background

Let us consider a single particle moving on the real line. The wave function for such a particle is a map $\psi : \mathbb{R} \longrightarrow \mathbb{C}$. This map evolves in time, but let us just assume time is frozen. The function $|\psi(x)|^2$is the probability density for the position of the particle. Thus, the probability that the position of the particle belongs to a set $E \subset \mathbb{R}$ is

$$\int_E |\psi(x)|^2 dx.$$

ψ should be normalized so that

$$\int_E |\psi(x)|^2 dx = 1.$$

It means ψ is a unit vector in Hilbert space $L^2(\mathbb{R})$.
We know from probability theory that if $|\psi|^2$ is the probability distribution the expectation value of the position will be

$$E(x) = \int_{\mathbb{R}} x|\psi(x)|^2 dx.$$

[1]Most of the background for quantum mechanics is based on [38]

$\psi(x)$, at any fixed time, encodes the probabilities for the particle's position. As it turns out the momentum is encoded in the oscillations of the wave function. The following proposition sheds more light at this idea.

Proposition 1.2.1. *(de Broglie's hypothesis) If the wave function of the particle has spatial frequency k, the momentum p of the particle is*

$$p = \hbar k$$

where $\hbar$ is Planck's constant.

Definition 1.2.2. For a particle moving in $\mathbb{R}$, the position and momentum operators X and P are defined by

$$X\psi(x) = x\psi(x)$$
$$P\psi(x) = -\imath\hbar\frac{d\psi}{dx}$$

Remark 1.2.3. Both these operators are unbounded, so they are defined on dense subspaces of $L^2(\mathbb{R})$, not the whole space.

Proposition 1. (The canonical commutation relation) *The position and momentum operators X and P satisfy following relation*

$$[X, P] = XP - PX = \imath\hbar I$$

, that is they don't commute. (Here I is the identity operator on $L^2(\mathbb{R})$.)

1.2.2 Axioms of quantum mechanics

In this section we consider axioms of quantum mechanics. There are two types of axioms, kinematics and evolutionary. The former ones are those that apply at one fixed point and the latter ones are those that govern the time evolution of a quantum system.
Axiom 1 The state of a quantum system is represented by a unit vector ψ in an appropriate Hilbert space $\mathcal{H}$. If ψ_1 and ψ_2 are two unit vectors in $\mathcal{H}$ with $\psi_2 = c\psi_1$ for some constant $c \in \mathbb{C}$, then ψ_1 and ψ_2 represent the same physical state.

Remark 1.2.4. In this axiom the unit vectors represent only the pure states of the theory. There is more general notion of a mixed state which we will discuss later.

Axiom 2 To each real-valued function f on the classical phase space there is associated a self-adjoint operator $\hat{f}$ on the quantum Hilbert space.

Remark 1.2.5. *Weyl quantization* is the standard approach to defining operator $\hat{f}$ for an arbitrary function f on the classical phase space, [38].

Remark 1.2.6. The classical phase space corresponding to a particle moving in $\mathbb{R}$ is $\mathbb{R}^2$. We can think of it as pairs (x, p) where x is the particle's position and p is its momentum. The quantum Hilbert space in this case is $L^2(\mathbb{R})$. In that case, if f is the position function, $f(x, p) = x$, then the corresponding operator $\hat{f}$ is the position operator X, given by multiplication by x. If $f(x, p) = p$, the momentum function, the associated operator $\hat{f}$ is the momentum operator $P = -\imath\hbar\frac{d}{dx}$.

Axiom 3 If a quantum system is in a state described by a unit vector $\psi \in \mathcal{H}$, The expectation value for a measurement of f is given by

$$\left\langle \psi, \hat{f}\psi \right\rangle.$$

Remark 1.2.7. If A is a self-adjoint operator on H and $\psi \in \mathcal{H}$ is a unit vector, the expectation value of A in the state ψ is denoted by $\langle A \rangle_\psi$ and is defined to be

$$\langle A \rangle_\psi = \langle A, A\psi \rangle$$

Axiom 4 The time-evolution of the wave function ψ in a quantum system is given by the Schrödinger equation

$$\frac{d\psi}{dt} = \frac{1}{\imath\hbar}\hat{H}\psi$$

Hear $\hat{H}$ is the operator corresponding to the classical Hamiltonian H as in Axiom 2.

Proposition 1.2.8. *Assume $\hat{H}$ is a self-adjoint operator on $\mathcal{H}$. Then the solution of the Schrödinger equation is*

$$\psi(t) = e^{-\frac{\imath\hat{H}t}{\hbar}}\psi(0)$$

Definition 1.2.9. If $\hat{H}$ is a Hamiltonian operator for a quantum system, the eigenvalue problem

$$\hat{H}\psi = E\psi, (E \in \mathbb{R})$$

is called time-independent or stationary Schrödinger equation.

The classical Hamiltonian for a particle with mass m moving in $\mathbb{R}$ is

$$H(x,p) = \frac{p^2}{2m} + V(x)$$

where V is the potential energy function. Now we may take

$$\hat{H}(X,P) = \frac{P^2}{2m} + V(X)$$

where the operator $V(X)$ is the multiplication by the potential energy function $V(x)$. $\hat{H}$ is called the Schrödinger operator. It's action on the state ψ is given by

$$\hat{H}\psi(x) = -\frac{\hbar^2}{2m}\frac{d^2\psi}{dx^2} + V(x)\psi(x)$$

.

1.2.3 Quantum composite systems and tensor product

I will define tensor product before introducing quantum composite systems.There are couples of ways to create new Hilbert spaces from old ones. In this section we describe the tensor product $\mathcal{H}_1 \otimes \mathcal{H}_2$ of two Hilbert spaces $\mathcal{H}_1$ and $\mathcal{H}_2$.

Definition 1.2.10. Let $\mathcal{H}_1$ and $\mathcal{H}_2$ be two Hilbert spaces. For each $\phi_1 \in \mathcal{H}_1$ and $\phi_2 \in \mathcal{H}_2$, let $\phi_1 \otimes \phi_2$ denote the conjugate bilinear form which acts on $\mathcal{H}_1 \times \mathcal{H}_2$ by

$$(\phi_1 \otimes \phi_2)(\psi_1, \psi_2) = \langle \psi_1, \phi_1 \rangle_1 \langle \psi_2, \phi_2 \rangle_2$$

Let E be the set of finite linear combinations of such conjugate linear forms; we define an inner product $\langle ., . \rangle$ on E by defining

$$\langle \phi \otimes \psi, \eta \otimes \mu \rangle = \langle \phi, \eta \rangle_1 \langle \psi, \mu \rangle_2$$

and extending by linearity to E, see [64].

Proposition 1.2.11. *The inner product $\langle .,. \rangle$ is well defined and positive definite, see [64].*

Definition 1.2.12. We define $\mathcal{H}_1 \otimes \mathcal{H}_2$ to be the completion of E under the inner product $\langle .,. \rangle$ defined above. $\mathcal{H}_1 \otimes \mathcal{H}_2$ is called the tensor product of $\mathcal{H}_1$ and $\mathcal{H}_2$.

Proposition 1.2.13. *If ϕ_k and ψ_l are orthonormal bases for $\mathcal{H}_1$ and $\mathcal{H}_2$ respectively, then $\phi_k \otimes \psi_l$ is an orthonormal basis for $\mathcal{H}_1 \otimes \mathcal{H}_2$, see [64].*

Proposition 1.2.14. *If H_1 and H_2 are bounded operators on $\mathcal{H}_1$ and $\mathcal{H}_2$ respectively, then $H_1 \otimes H_2$ is the unique bounded operator on $\mathcal{H}_1 \otimes \mathcal{H}_2$, such that*

$$(H_1 \otimes H_2)(\phi_1 \otimes \phi_2) = (H_1\phi)(H_2\phi)$$

for all $\phi_1 \in H_1$ and $\phi_2 \in H_2$

Proposition 1.2.15. *Suppose that (X_1, μ_1) and (X_2, μ_2) are σ-finite measure spaces. Then there is a unique isomorphism*

$$p : L^2(X_1, \mu_1) \otimes L^2(X_2, \mu_2) \longrightarrow L^2(X_1 \times X_2, \mu_1 \otimes \mu_2)$$

so that $f \otimes g \longmapsto fg$.

Axiom 5 The Hilbert space for a composite system consists of two subsystems $\mathcal{H}_1$ and $\mathcal{H}_2$ is the Hilbert tensor product $\mathcal{H}_1 \otimes \mathcal{H}_2$, see [38].

Proposition 1.2.16. *Suppose H_1 and H_2 are self-adjoint operators on $\mathcal{H}_1$ and $\mathcal{H}_2$ respectively. Following operators are self-adjoint as well*

$$H_1 \otimes H_2 \quad \text{and} \quad H_1 \otimes I + I \otimes H_2,$$

as well as

- $\sigma(H_1 \otimes H_2) = \overline{\{\lambda_1\lambda_2 | \lambda_i \in \sigma(H_i)\}}$
- $\sigma(H_1 \otimes I + I \otimes H_2) = \overline{\{\lambda_1 + \lambda_2 | \lambda_i \in \sigma(H_i)\}}$
  For a proof look at [75]

Axiom 6 Suppose $\mathcal{H}_i$, $i = 1, 2$ are the Hilbert spaces for two quantum systems, with Hamiltonians H_i. Then the Hamiltonian for the non-interacting composite system is

$$H_1 \otimes I + I \otimes H_2.$$

Generally, the two subsystems of a composite quantum system will interact, in this case the Hamiltonian for the composite system is

$$H = H_1 \otimes I + I \otimes H_2 + H_{int},$$

where H_{int} is an *interaction term.*

1.2.4 The physics notation

In quantum mechanics, it is common to use the Dirac notation introduced by P. Dirac in 1930's.

1. A vector $\psi \in \mathcal{H}$ is denoted by $|\psi\rangle$ and referred to as a ket. A continuous linear functional on $\mathcal{H}$ is called a bra and denoted by $\langle\phi|$. $< \phi|\psi >$ is referred to as the bracket of two vectors $\phi, \psi \in \mathcal{H}$ by applying the bra $\langle\phi|$ to the ket $|\psi\rangle$, namely the inner product of ϕ and ψ.

2. If A is an operator on $\mathcal{H}$ and $\phi \in \mathcal{H}$ the linear functional $\langle\phi| A$ is the linear map $\psi \longmapsto \langle\phi| A |\psi\rangle$. There are two different ways of thinking about this notation. we can think of it as the linear functional $\langle\phi| A$ applied to the vector $|\psi\rangle$, or as the linear functional $\langle\phi|$ applied to the vector $A|\psi\rangle$.

3. For any ϕ and $\psi \in \mathcal{H}$, $|\phi\rangle\langle\psi|$ denotes the following linear operator on $\mathcal{H}$. Let $\chi \in \mathcal{H}$,

$$(|\phi\rangle\langle\psi|)(\chi) = |\phi\rangle\langle\psi|\,\chi\rangle = \langle\psi|\,\chi\rangle|\phi\rangle.$$

4. Suppose the orthonormal eigen-basis of $\hat{H}$ is $\{\psi_n\}$. It is common to express the decomposition of a general vector in the basis $\{\psi\}$ via the identity operator

$$I = \sum_n |n\rangle\langle n|.$$

Here, ψ_n is represented as $|n\rangle$ and $|n\rangle\langle n|$ is the orthogonal projection onto the one dimensional subspace spanned by the vector $|n\rangle$.

5. If $|\Phi_c\rangle$ and $|\Psi_c\rangle$ be in $\mathcal{H}_1 \otimes \mathcal{H}_2$ we can show them as

$$|\Phi_c\rangle = \sum_{k,l} s_{kl}|\phi_k\rangle|\psi_l\rangle, \quad |\Psi_c\rangle = \sum_{m,n} z_{mn}|\phi_m\rangle|\psi_n\rangle$$

then

$$< \Phi_c, \Psi_c >= \sum_{m,n,k,l} z_{mn}\bar{s}_{kl} < \phi_k, \phi_m >< \psi_l, \psi_n > .$$

It follows that if $\phi_m \in \mathcal{H}_1$ and $\psi_n \in \mathcal{H}_2$ are orthonormal bases, then

$$< \Phi_c, \Psi_c >= \sum_{m,n} z_{mn}\bar{s}_{mn}.$$

1.2.5 Quantum Harmonic Oscillator[2]

By a quantum harmonic oscillator we mean a system consisting of one particle on the line whose dynamics is determined via the following Hamiltonian

$$\hat{H} = \frac{1}{2m}\left(P^2 + (m\omega X)^2\right).$$

Here, m is the mass of the particle, ω is the frequency of the corresponding classical harmonic oscillator (mass attached to a spring), P is the momentum and X is the position operator. Both P and X are self- adjoint operators and satisfy $[X, P] = \iota\hbar I$. We now introduce the lowering (creation) and it's adjoint, the rising (annihilation), operators given by

$$a = \frac{m\omega X + \iota P}{\sqrt{2\hbar m\omega}}$$

and

$$a^* = \frac{m\omega X - \iota P}{\sqrt{2\hbar m\omega}}$$

respectively. Thus

$$a^*a = \frac{1}{2\hbar m\omega}((m\omega X)^2 + P^2 + \iota m\omega[X, P])$$

[2]This subsection is mostly based on [26].

$$= \frac{1}{\hbar\omega}\frac{1}{2m}(P^2 + (m\omega X)^2) - \frac{1}{2}I.$$

From this we obtain

$$\hat{H} = \hbar\omega(a^*a + \frac{1}{2}I) \tag{1.2.1}$$

The derivation consists of following steps: First

$$[X, P] = \iota\hbar I.$$

Second in the world of noncommuting operators

$$(A - B)(A + B) = A^2 - B^2 + [A, B].$$

It is easy to see that

$$[a, a^*] = I$$

and from this compute that

$$[a, a^*a] = a$$

$$[a^*, a^*a] = -a^*.$$

Since $(a^*a)^* = a^*a^{**}$, a^*a is self-adjoint. This operator is also non-negative because

$$\langle\psi, a^*a\psi\rangle = \langle a\psi, a\psi\rangle \geqslant 0$$

for all ψ.

Theorem 1.2.1. *If ψ_0 is a normalized vector with the property that $a\psi_0 = 0$, then*

$$\psi_n = \frac{1}{\sqrt{n!}}(a^*)^n\psi_0, \quad n \geqslant 0$$

satisfy the following relations for all $n, m \geqslant 0$:

$$\begin{aligned} a^*\psi_n &= \sqrt{n+1}\psi_{n+1} \\ a\psi_n &= \sqrt{n}\psi_{n-1} \\ a^*a\psi_n &= n\psi_n \\ \langle\psi_n, \psi_m\rangle &= \frac{1}{\sqrt{n!m!}}\delta_{n,m} \end{aligned}$$

What we have consider so far is an algebraic approach to the study of the harmonic oscillator. we are now going to look at that from an analytical point of view.
To simplify our analysis, we change position variable x to

$$\tilde{x} = \sqrt{\frac{m\omega}{\hbar}}x$$

By a simple calculation we obtain the following expressions for the creation and annihilation operators

$$a = \frac{1}{2}\left(\tilde{x} + \frac{d}{d\tilde{x}}\right)$$
$$a^* = \frac{1}{2}\left(\tilde{x} - \frac{d}{d\tilde{x}}\right)$$

Using this one can solve the equation $a\psi_0 = 0$ explicitly, and obtain

$$\psi_0 = \sqrt[4]{\frac{\pi m\omega}{\hbar}}\exp\{-\frac{m\omega}{2\hbar}x^2\} \tag{1.2.2}$$

which is called ground state.

Theorem 1.2.2. *The excited state ψ_n of the harmonic oscillator is given by*

$$\psi_n = H_n\psi_0$$

where H_n is the Hermite polynomial given by following formula

$$H_n(\tilde{x}) = (-1)^n e^{\tilde{x}^2}\frac{d^n}{d\tilde{x}^n}e^{-\tilde{x}^2}, \quad n = 0, 1, 2, \cdots.$$

Theorem 1.2.3. *The functions*

$$\begin{aligned}\psi_n(x) &= H_n(\tilde{x})\psi_0(\tilde{x}) \\ &= H_n\left(\sqrt{\frac{m\omega}{\hbar}}x\right)\sqrt[4]{\frac{\pi m\omega}{\hbar}}\exp\{-\frac{m\omega}{2\hbar}x^2\}\end{aligned}$$

form an orthonormal basis for the Hilbert space $L^2(\mathbb{R})$.

Theorem 1.2.4. *$E_n = \hbar\omega\left(n + \frac{1}{2}\right)$ and $\{\psi_n\}$ are the eigenvalues and the eigenfunctions of the harmonic oscillator.*

Now we are interested in representing the harmonic oscillator operator in two spaces $\ell^2(\mathcal{N})$ and the space of entire analytic functions (Segal-Bargmann space) $\mathcal{D}$
Since eigenvectors of a harmonic oscillator span the Hilbert space, so if $\psi \in \mathcal{H}$

$$\psi = \sum_n C_n \frac{(a^*)^n}{\sqrt{n!}}\psi_0 \quad \sum_n |C_n|^2 < \infty,$$

where ϕ_0 is given by 1.2.2. Each vector $\phi \in \mathcal{H}$ is uniquely determined by the coefficient sequence $\{C_n\}$.
If $\psi \longleftrightarrow \{B_n\}$, then

$$\langle \psi, \phi \rangle = \sum_n B_n \bar{C}_n.$$

After calculations

$$\begin{aligned} a\phi &= \sum_n \sqrt{n+1} C_{n+1} \frac{(a^*)^n}{\sqrt{n!}}\psi_0 \\ a^*\phi &= \sum_n \sqrt{n} C_{n-1} \frac{(a^*)^n}{\sqrt{n!}}\psi_0 \end{aligned}$$

In the basis the operators a and a^* have matrix representations

$$a = \begin{pmatrix} 0 & \sqrt{1} & 0 & 0 & \cdots \\ 0 & 0 & \sqrt{2} & 0 & \cdots \\ 0 & 0 & 0 & \sqrt{3} & \cdots \\ \vdots & \vdots & \vdots & \vdots & \vdots \end{pmatrix}$$

and

$$a^* = \begin{pmatrix} 0 & 0 & 0 & 0 & \cdots \\ \sqrt{1} & 0 & 0 & 0 & \cdots \\ 0 & \sqrt{2} & 0 & 0 & \cdots \\ 0 & 0 & \sqrt{3} & 0 & \cdots \\ \vdots & \vdots & \vdots & \vdots & \vdots \end{pmatrix}$$

The eigenvectors of the operator H in this representation have the form

$$\psi_i = \begin{pmatrix} 0 \\ \vdots \\ 1 \\ 0 \\ \vdots \end{pmatrix}$$

Where the ith element is 1.

Now, the harmonic oscillator Hamiltonian, momentum and position operators will be given as

$$H = \hbar\omega \begin{pmatrix} \frac{1}{2} & 0 & 0 & 0 & \cdots \\ 0 & \frac{3}{2} & 0 & 0 & \cdots \\ 0 & 0 & \frac{5}{2} & 0 & \cdots \\ 0 & 0 & 0 & \frac{7}{2} & \cdots \\ \vdots & \vdots & \vdots & \vdots & \vdots \end{pmatrix},$$

$$P = \frac{\sqrt{\hbar m\omega}(a - a^*)}{\iota\sqrt{2}} = \frac{\sqrt{\hbar m\omega}}{\iota\sqrt{2}} \begin{pmatrix} 0 & \sqrt{1} & 0 & 0 & \cdots \\ -\sqrt{1} & 0 & \sqrt{2} & 0 & \cdots \\ 0 & -\sqrt{2} & 0 & \sqrt{3} & \cdots \\ 0 & 0 & -\sqrt{3} & 0 & \cdots \\ \vdots & \vdots & \vdots & \vdots & \vdots \end{pmatrix}$$

and

$$X = \frac{\sqrt{\hbar}(a + a^*)}{\sqrt{2m\omega}} = \frac{\sqrt{\hbar}}{\sqrt{2m\omega}} \begin{pmatrix} 0 & \sqrt{1} & 0 & 0 & \cdots \\ \sqrt{1} & 0 & \sqrt{2} & 0 & \cdots \\ 0 & \sqrt{2} & 0 & \sqrt{3} & \cdots \\ 0 & 0 & \sqrt{3} & 0 & \cdots \\ \vdots & \vdots & \vdots & \vdots & \vdots \end{pmatrix}.$$

Another representation where H is diagonal is constructed as follows. Let

$$\mathcal{D} = \{F; \quad F \text{ is an entire function on } \mathbb{C} \text{ and } |F|^2 = \int |F(z)|^2 e^{-|z|^2} < \infty\}$$

with the inner product

$$\langle f, g\rangle = \frac{1}{\pi}\int f(z)g(\bar{z})e^{-|z|^2}d\mu(z) \quad f, g \in \mathcal{D}$$

where $d\mu(z) = dxdy$. $\mathcal{D}$ is a Hilbert space with the orthonormal basis

$$f_n(z) = \frac{z^n}{\sqrt{n!}} \quad n = 0, 1, 2, \cdots.$$

The following correspondence indicates that $\ell^2 \simeq \mathcal{D}$,

$$\ell^2 \ni c = \{c_n\} \longmapsto f(z) = \sum_n c_n f_n(z) \in \mathcal{D}.$$

The isomorphism between ℓ^2 and $\mathcal{D}$ leads to the following representation of a and a^*

$$a^* = z, \quad a = \frac{d}{dz}.$$

Subsequently

$$H = \hbar\omega\left(z\frac{d}{dz} + \frac{1}{2}\right).$$

1.3 Quantum mechanics in electronics

One of the main objects of modern electronics is to fabricate nano-transistors . Since their dimensions are getting tinier day by day employing quantum mechanics in order to model the devices is inevitable.

1.3.1 The quantum dot

It is necessary to explain semiconductors before any discussion of quantum dots. A semiconductor is a material with electrical conductivity between those of metals and insulators. Typically, semiconductors are made of silicon (Si), germanium (Ge) or gallium arsenide (GaAs). These materials have many important technological applications. They are the basic constituents of electronic devices such as computers, telephones and so on. Semiconductors devices include transistors, diodes and so on.

Band theory of semiconductors An isolated silicon atom possesses 14 electrons with electron configuration $1s^2 2s^2 2p^6 3s^2 3p^2$ as shown in figure 1.1.

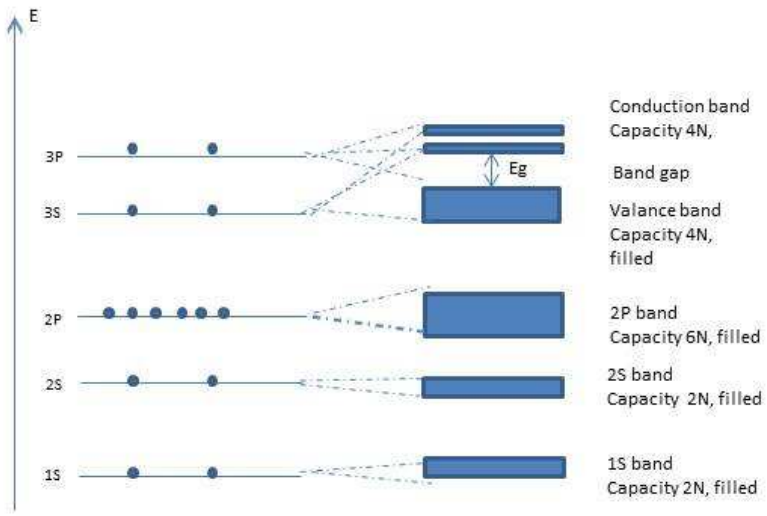

Figure 1.1: The occupation of the energy levels in an isolated silicon atoms and the energy bands in a silicon crystal.

If we plot the energies of $3s$ and $3p$ energy levels for N silicon atoms as a function of inter-atomic distance we observe that the two sets of energy levels interact, as shown in Figure 1.2. At the level of exiton Bohr radius the states split up into two bands which are each mixture of 3s-and 3p-like states. The lower energy band possesses $4N$ electrons and is known as the valance band. Valance band corresponds to electrons which are involved in forming covalent bonds of crystal. The electrons in the upper band are relatively free and so can take part in electrical conduction. This band possesses $4N$ electrons as well and is called conduction band. These two bands are separated by an energy range in which there are no allowed electron energy levels. This is the band gap and we denote its energy space by E_g. The most significant difference between metals and non-metals is the existence of the band gap. In metals there is no band gap so the highest occupied band is only partially filed, whereas in non-metals the highest occupied states (at $T = 0$ K, or absolute zero) are separated from lowest vacant states by a band gap which is a region of forbidden energy. Excitation of electrons from the valance band through the gap into the conduction band is mainly responsible for electrical conduction.

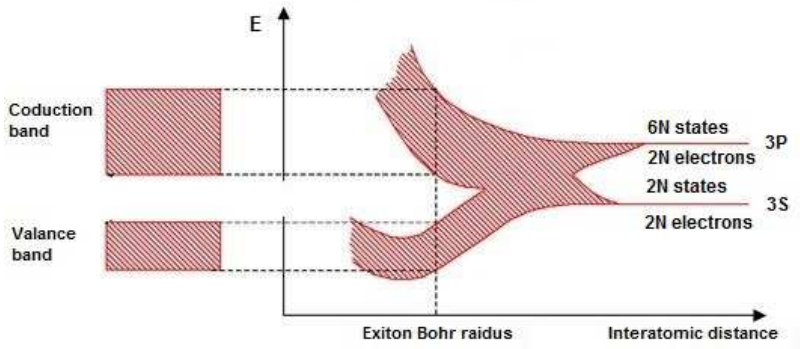

Figure 1.2: The energy levels of the $3s$ and $3p$ states for a group of N silicon atoms as a function of inter-atomic distance[3].

According to this fact one can explain the difference between conductivity in metals and non-metals. Once one applies an electric field to the material the electron in metals can gain a small amount of energy by moving to a nearby unoccupied state. In contrast to this in non-metals, because of presence of energy gap between valance band and conduction band, this process can not occur. Therefore these materials are electrical insulators. If the band gap is sufficiently small and $T > 0K$, there is a chance to find some electrons in the conduction band, so the material conducts the electricity. This is the key point to understanding the difference between semiconductors and insulators. The conductivity is dependent on temperature and the band gap energy. In order to explain this fact quantitatively we need to introduce the Fermi-Dirac distribution.

Definition 1.3.1. The probability that a state with energy E is occupied at temperature T is given by Fermi-Dirac distribution

$$f(E) = \frac{1}{1 + \exp(\frac{E-E_F}{K_B T})} \quad 0 \leqslant E < \infty$$

where E_F is the Fermi energy that is the energy for which the probability of occupation is $\frac{1}{2}$.

Now, the question is at what energy for non-metals the probability is one-half. It has been proven that the Fermi energy is located at the center of the band gap, see [77]. So

[3]Partially adopted from google images

$E - E_f = \frac{E_g}{2}$. Consequently using previous equation implies

$$f(E) = \frac{1}{1 + \exp(\frac{E_g}{2K_BT})}.$$

Since the exponential term of previous equation is much larger than 1, therefore

$$f(E) \approx \exp \frac{-E_g}{2K_BT}.$$

Consequently the concentration of electron in conduction band increases as the temperature rises up.

So far we have seen that how electrons contribute to the electrical conductivity. However, they are not the only contributors. Once the electron get excited to the conduction band it leaves behind electron hole, or unoccupied state in the valance band. Then a neighbouring electron move to file this hole, so it leaves another hole in a place just come from, therefore we have a sequence of events in which an electron moves towards the opposite side of crystal and in this way the hole appear to move. In this regard the hole behaves as if it was actual positively charged particle. Since these two types of particles have opposite charges, the total current is equal to the sum of the electron and hole (*exciton*) current, see [77].

Research in semiconductors has taken on new dimensions, two, one, and zero. Electron in new electronic devices can be confined to a mathematical point that is called for the first time by Mark Reed "quantum dot"[66, 65]. Now question is, how is it possible to make this mathematical object in a real, three dimensional material? Quantum mechanics answers this question.

If an electron is confined in a small enough three dimensional box it exhibits properties similar to a particle confined in an infinite quantum well that its energy is discrete. We observed that its lower energy is not zero compared to a free quantum particle. Therefore size quantization is a result of confinement. Quantization effects become apparent when the dimensions of the confining region are comparable to the De Broglie wavelength of the charge carriers (electrons and holes). The De Broglie wave length is $\lambda \simeq \frac{h}{\sqrt{2m^* K_B T}}$, where h and K_B are the Planck's and Boltzmann's constants, T the temperature and m^* the

effective mass of the excitons (electron-hole) in the semiconductor. At low temperature λ is of the order 10 to 100 nm. Instead of considering De Broglie wave length for electrons and holes separately, it is reasonable to describe a quantum dot as a region of space in a semiconductor whose size is on the order of the exciton Bohr radius. The exciton Bohr radius is considerably larger than the hydrogen Bohr radius which is about 0.53 Angstrom or 0.053 nm,[63].

Quantum dot modelling A simple model for a quantum dot should incorporate two different types of potential. First, a confining potential which traps the electrons into the dot and, second, the interaction potential which characterizes the interaction between trapped electrons.

- ***The confining potential*** In order to model a quantum dot we need a potential to confine electrons inside the dot. This potential does the job that in real atom is done by the nucleus. Some experimental studies have shown that , the harmonic oscillator potential, $\sum_{i=1}^{n} \frac{1}{2} m\omega^2 (|X^{(i)}|)^2$ where $X^{(i)} = (x^{(i)}, y^{(i)}, z^{(i)})$, is a good candidate [2].

- ***The interaction potential*** In quantum mechanics the Schrödinger operator for a system of n pairwise interacting particles in an external field is expressed via

$$H = \sum_{i=1}^{n} \frac{-1}{2m} \Delta_i + \sum_{i=1}^{n} V(X^{(i)}) + \sum_{i<j}^{n} U(X^{(i)} - X^{(j)})$$

  [26]. The first term is the kinetic energy operator of the system of particles (electrons, the second term describes the interaction of the particles with external field such as electro magnetic field, and the third term is the interaction of the particles with each other. m is the mass of the particles.

  Usually, it is assumed the interaction between the electron in the quantum dot is the Coulomb interaction. Since electron in the quantum dot trapped by harmonic oscillator potential the Schrödinger operator is

$$\sum_{i=1}^{n} \left(\frac{-\hbar^2}{2m} \Delta_i^2 + \frac{1}{2} m\omega^2 (|X^{(i)}|)^2 \right) + \frac{q^2}{4\pi\epsilon_0 \epsilon} \sum_{i<j}^{n} \frac{1}{|X^{(i)} - X^{(j)}|}$$

  where q is the charge of the electron, ϵ_0 and ϵ are dielectric constants. In this approach, the external field such as electro magnetic field has been neglected.

1.3.2 The quantum-effect devices

Fabricating nano-transistors is one of the main objects of modern electronics. Since their dimensions are getting tinier day by day invoking quantum mechanics becomes necessary. There are two different quantum effect devices, field effect transistors (FET) and single electron transistors (SET). Each of these devices has its own advantages and disadvantages [71].

- ***The FET*** As it is illustrated in figure 1.3 a field effect transistors (FET) consists of three main parts, the source, the channel and the drain that one can assume them as three quantum wells [73]. A FET is a transistor that uses an electric field to control the conductivity of a channel of one type of charge carrier (electron-hole) in a semiconductor material. I give a simplistic picture of electron transport through this FET via a three-infinite-quantum-well model to analyse this simple three-partite junction and then in next section a sophisticated model will be introduced.

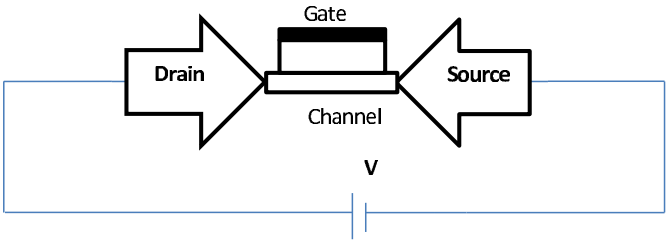

Figure 1.3: A FET .

First I will briefly explain the infinite quantum well. Recall that the time independent Schrödinger equation is

$$E\psi(x) = -\frac{\hbar^2}{2m}\frac{d^2\psi(x)}{dx^2} + V(x)\psi(x).$$

Now, assume a particle is confined to an interval $[0, L]$ which $V = 0$ in there and $V = \infty$ outside of this interval So, the above equation reduces to following one

$$\frac{d^2\psi(x)}{dx^2} + k^2\psi(x) = 0$$

where

$$k = \frac{\sqrt{2mE}}{\hbar}$$

with the boundary conditions $\psi(0) = \psi(L) = 0$. Solutions are readily found in the form

$$\psi(x) = A\sin(kx) \qquad k = k_n = \frac{n\pi}{L} \quad n = 1, 2, 3, \cdots.$$

Now since $k_n = \frac{\sqrt{2mE}}{\hbar} = \frac{n\pi}{L}$

$$E = \mathcal{E}_n = \frac{\hbar^2\pi^2}{2mL^2}n^2 \quad n = 1, 2, 3, \cdots.$$

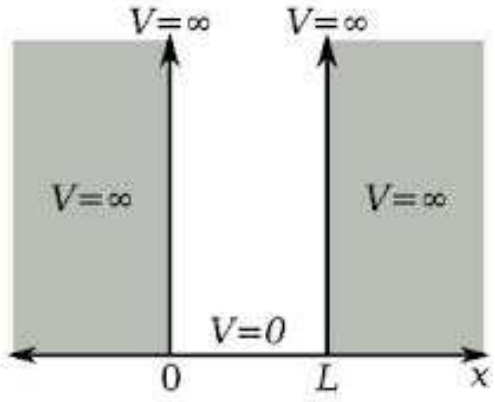

Figure 1.4: An infinite well.

Since $1eV = 1.6 \times 10^{-19}J$ and $J = \frac{Kg.m^2}{s^2}$ then for an infinite well with length L nm (nano-meter).

$$\mathcal{E}_n = \frac{\hbar^2\pi^2}{2mL^2}n^2 = \frac{(1.054 \times 10^{-34})^2(3.14159)^2}{2(9.11 \times 10^{-31})(L \times 10^{-9})^2}n^2\left[\frac{J^2s^2}{Kg.m^2}\right]$$

$$= .6 \times 10^{-19}\frac{eV}{1.6 \times 10^{-19}}n^2 = 0.375(\frac{n}{L})^2eV.$$

Therefore for a well with length $2L$ nm

$$\mathcal{E}_n = 0.093(\frac{n}{L})^2eV.$$

The figure 1.3 illustrates a semiconductor field-effect transistor, or FET.

An infinite well which is separated in three parts or three quantum wells is depicted in figure1.5. The middle well is L nm like above infinite quantum well. The right and left wells are 2L nm. It is common to think of the right well as the *source*, the left well as the *drain* and the middle well as the *channel*.

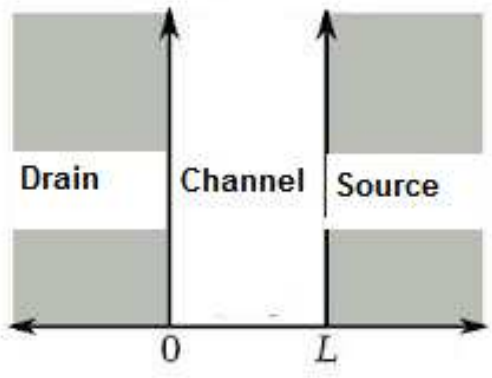

Figure 1.5

It is interesting to ask how a particle moves from the source to the drain. Momentarily, assume the partitions are not infinite. And let a particle in the right well be in its second eigenstate (n=2) so its energy is $\mathcal{E}_2 = 0.093 \times 4(\frac{1}{L})^2 eV$ and let the middle well (The channel) be in its ground state (n=1) so its energy is $\mathcal{E}_1 = 0.375(\frac{1}{L})^2 eV$. Thus the particle can tunnel into the channel and from channel into the drain.

- ***The SET***[4] A SET can be considered as a FET whose channel consists of a low capacitance quantum dot coupled to the source and contact by two tunnel junctions and "capacitively coupled" to the gate which is used to control the transfer of single electron from source to drain [71]. The fundamental concept behind the SET is single electron transfer or "*single electronics*" [50, 51]. It can be explained by

[4]Most of this section is based on [71]

assuming a small metallic sphere which the net charge on it is zero. If a single electron approaches to the sphere it will get attracted by the sphere. So in this case the charge of the sphere is negative. This negative charge produces an electric field around the sphere that repels any other electron.

The phenomenon of single electron transfer is comprehensible provided the concept about the movement of electronic charge through a conductor is clear. Due to free electrons in a conductor the current flows through it. Since the charge transferred through the conductor may have any value it is not quantized. In order to quantize the charge transfer, a tunnel junction is located in a conductor. Therefore, the flow of electrons will be restricted. Now, if an electron tunnels through the junction, the charge will be accumulated at the tunnel junction. An individual electron can be forced to transfer by applying a high bias voltage across the junction.

The charging and discharging of the tunnel junction and thermal fluctuations are correlated. Since the the high temperature can disturb quantization effect the Coulomb energy must be grater than thermal fluctuation, $(E_c = \frac{e^2}{2c} > K_B T)$, where c is the capacitance of the junction and e is the electron charge. This is the required condition for single electron phenomenon. Unlike the FET, the SET is based on a quantum mechanic phenomenon known as the tunnelling effect. This effect may be observed when two metallic electrodes are separated by an insulator named tunnel junction. This three-partite device transfer electrons from source to drain on by one.

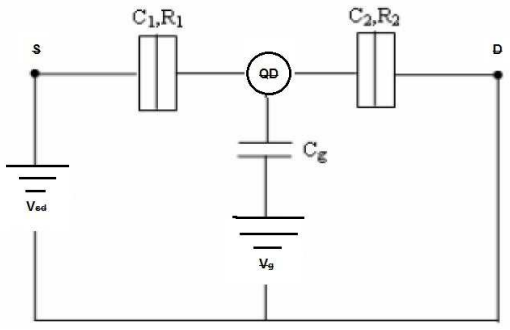

Figure 1.6: SET circuits with one QD.

Quantum dot is a small conducting island that contain a tunable number of electrons. As shown in figure 1.6 a gate voltage is used to control one by one electron transfer. One tunnel junction is located between source and QD and another one is located between QD and drain with tunnel capacitances (c_1, c_2) and tunnel resistances (R_1, R_2) respectively. The capacitance of the QD, C, is the total sum of the capacitances of tunnel junctions and gate capacitance. So the coulomb energy or electrostatic energy of the QD is $E_C = \frac{e^2}{C}$. This is the repelling energy of previous electron present in the QD to the next electron approaching towards the QD. Now, since the smaller QD has smaller capacitance the blockaded energy E_C is high enough to prevent simultaneous movement of electrons. Therefore, the electrons pass on by one. This phenomenon is called "*Coulomb blockade*".

In FETs, the drain current depends on the number of electrons passing through the channel. Hence, the more electrons in the channel, the larger the drain current. Therefore V_g/I_d diagram is monotonic. In case of SETs, the drain current does not depend on the number of electrons in the channel. Therefore V_g/I_d diagram is periodic, see [71].

1.3.3 Electron transport[5]

The most remarkable characteristic of modern technology is its emphasis on miniaturization. Electronics is the most striking example where technological progress has come from reductions in the size of transistors. The tinier the transistor, the more transistors can be etched in a chip. Classical models to describe transistors behaviour have been abandoned. For example, it has been shown that electrons in modern transistors travel "ballistically". That is, they do not collide with any component of the silicon channel unlike "diffusive" conductors in which electron takes a random walk from the source to the drain. Therefore, scientists have chosen the "bottom-up" approach rather "top-down" approach, from large complicated conductors down to atoms, to analyse these transistors.

[5]Most of this section is based on [18]

Since quantum mechanics starts from atoms not from bulk solids it is the cornerstone of bottom-up approach.

Transport through a channel involves two different types of processes, frictionless transfer and heat generation. The first involves mechanics of the type described by Newton's laws or the Schrödinger equation. The second described by laws of thermodynamics. A proper description of electron transport in an electronic device depends on methods of non-equilibrium statistical mechanics which integrates mechanics with thermodynamics. Historically, there are two different models to describe electron transport in an electronic device, semi-classical model and quantum models.

- **Boltzmann transport equation (BTE)**, results from integrating Newtonian mechanics with heat generating or entropy processes, is accepted as the base of semi-classical transport theory.

- **The non-equilibrium Green function (NEGF)** method integrating quantum dynamics with heat generating processes in order to gives a full description of quantum transport.

The former one introduced by Boltzmann over a century ago and the latter one introduced in 1960's by Keldysh [44], Martin and Schwinger [54].

Next, I will describe briefly the two approaches for one level case. This method has been developed by Supriyo Datta [16, 18, 17].

- *The semi-classical approach*: Assume we have a channel that consists of only one level connected to two contacts, with two different Fermi-Dirac distributions

$$f_1(E) = \frac{1}{1+\exp(\frac{E-\mu_1}{kT})} \quad f_2(E) = \frac{1}{1+\exp(\frac{E-\mu_2}{kT})}$$

  where μ_i is the electrochemical potential of contacts (the value at which the probability of occupation of the level is $\frac{1}{2}$), $k = 1.38\times10^{-23} Joule/K$ is Boltzmann constant and T (Kelvin) is temperature.

  Remark 1.3.2. Fermi-Dirac distribution expresses the probability that a quantum state at energy E is occupied.

Now, what makes electrons flow through the channel is the difference between f_1 and f_2 and the current through the channel is

$$I(E) = q\frac{\nu_1\nu_2}{\nu_1+\nu_2}(f_1(E) - f_2(E))$$

where $q = 1.6 \times 10^{-19} coul.$ is the electronic charge and ν_i represent the rates (per second) at which an electron escapes into the contacts.

- *The quantum approach*: By introducing contacts into the time dependent Schrödinger equation 1.2.2, we obtain

$$\iota\hbar\frac{d}{dt}\psi = (\varepsilon - \iota\frac{\gamma_1+\gamma_2}{2})\psi$$

where $\frac{\gamma_i}{\hbar} = \nu_i$. And the corresponding time independent Schrödinger equation is

$$E\phi = (\varepsilon - \iota\frac{\gamma_1+\gamma_2}{2})\phi.$$

This equation has a solution $\phi = 0$, so at steady-state there are no electrons occupying the level because we have not included the source term s_1, that is the rate at which electrons try to enter from the source into the channel. Therefore,

$$E\phi = (\varepsilon - \iota\frac{\gamma_1+\gamma_2}{2})\phi + s_1.$$

Subsequently

$$\phi = [(E-\varepsilon) + \iota\frac{\gamma}{2}]^{-1}s_1$$

where $\gamma = \gamma_1 + \gamma_2$. And $[(E-\varepsilon) + \iota\frac{\gamma}{2}]^{-1}$ is the retarded Green's function. Therefore the number of electrons passing through this one level channel is

$$\phi\phi^* = [(E-\varepsilon) + \iota\frac{\gamma}{2}]^{-1}s_1s_1^*[(E-\varepsilon) - \iota\frac{\gamma}{2}]^{-1} = [(E-\varepsilon)^2 + (\frac{\gamma}{2})^2]^{-1}s_1s_1^*.$$

Considering another inflow source term s_2 one can obtain

$$\phi\phi^* = [(E-\varepsilon)^2 + (\frac{\gamma}{2})^2]^{-1}(s_1s_1^* + s_2s_2^*).$$

which is the one dimensional analogue of NEGF.

Remark 1.3.3. Since the extra terms $s_1 s_2^* + s_2 s_1^*$ are never observed experimentally we don't take them into the account, see [18].

By integrating the total number of electron over all energies

$$\begin{aligned}\int_{-\infty}^{\infty} \phi\phi^* dE &= \int_{-\infty}^{\infty} \frac{(s_1 s_1^* + s_2 s_2^*)}{(E-\varepsilon)^2 + (\frac{\gamma}{2})^2} dE \\ &= \int_{-\infty}^{\infty} \frac{\frac{\gamma}{2\pi}}{(E-\varepsilon)^2 + (\frac{\gamma}{2})^2} (f_1(E) - f_2(E)) dE \\ &= \int_{-\infty}^{\infty} D(E)(f_1(E) + f_2(E)) dE\end{aligned}$$

where $2\pi(s_1 s_1^* + s_2 s_2^*) = \gamma(f_1(E) + f_2(E))$ and $D(E)$is density of states[18]. Now after considering some assumptions [18] the current through the channel would be

$$I = I_{in} - I_{out} = \frac{q}{\hbar} \frac{\gamma_1 \gamma_2}{\gamma_1 + \gamma_2} \int_{-\infty}^{\infty} D(E)(f_1(E) - f_2(E)) dE$$

Remark 1.3.4. According to quantum mechanics coupling the channel to the contacts spreads a single energy level into a state that is distributed in energy. This is a consequence of uncertainty principle $\gamma t \geqslant h$ which relates the time that electron spends in a level to the uncertainty γ in the energy. The stronger the coupling, the shorter the time and the larger the broadening [18].

Remark 1.3.5. According to uncertainty principle the process of coupling the device to the contacts spreads a single energy level into a state that is distributed in energy, so this phenomenon is the property of quantum picture which semi-classical picture misses.

Above argument can be extended to more than one energy level [18]. Assume $[H]$ is a $n \times n$ Hamiltonian matrix whose eigenvalues give the n energy levels. For an n level channel, the wave function $\{\psi\}$ and source term $\{s_1\}$ are $n \times 1$ vectors and the Schrödinger equation looks like

$$E\{\phi\} = [H + \Sigma_1 + \Sigma_2]\{\phi\} + \{s_1\}$$

where Σ_i are $n \times n$ non-Hermitian matrices which $\Gamma_i = \iota[\Sigma_i - \Sigma_i^\dagger]$ play the roles of γ_i in the one-level case. One can write above equation as

$$\{\phi\} = [EI - H - \Sigma]^{-1}\{s_1\}$$

where

$$G(E) = [EI - H - \Sigma]^{-1}$$

is the retarded Green's function which it is shown by G^R. The matrix electron density, the NEGF, define as

$$G^n = 2\pi\{\phi\}\{\phi\}^* = 2\pi G^R\{s_1\}\{s_1\}^*(G^R)^*.$$

Assuming $2\pi\{s_1\}\{s_1\}^* = \Gamma_1$

$$G^n = G^R\Gamma_1(G^R)^*.$$

This is NEGF for single source term. For two sources

$$G^n = G^R\Sigma^{in}(G^R)^*$$

where $\Sigma^{in} = \Gamma_1 f_1(E) + \Gamma_2 f_2(E)$ as well as f_1 and f_2 are the Fermi function of source and drain respectively. If both f_1 and f_2 are equal to one then all states are occupied, therefore the matrix electron density becomes equal to the matrix density of states, called the spectral function, see [18]. Accordingly the matrix density of states is

$$A = G^R\Gamma(G^R)^*$$

where $\Gamma = \Gamma_1 + \Gamma_2$. after some calculation [18]

$$A = \iota[G^R - (G^R)^*].$$

The system's conductivity is determined by the quantity $trace(A)$. This is the main observation of NEGF theory. And the current flowing through the channel would be

$$I = \frac{q}{2\pi\hbar}\int_{-\infty}^{\infty} Trace(\Gamma_1 G^R\Gamma_2(G^R)^*)(f_1(E) - f_2(E))$$

where $T = Trace(\Gamma_1 G^R\Gamma_2(G^R)^*)$ is called the transition function.

1.4 The Jaynes-Cummings model[6].

Two fundamental models of quantum mechanics, are the two level system and harmonic oscillator. If one combines these two into a bipartite system they can get several inter-

[6]This section is based on [72]

esting models, which one of them is Jaynes-Cummings (JC). Jaynes-Cummings model was introduced for describing the interaction between a two level atom and a quantized electromagnetic field. This model has so many applications in modern science and technology.

The Jaynes-Cummings model is based on a Hamiltonian which assumes the following form:

$$H = I \otimes H_F + H_a \otimes I + H_{int} : \quad \mathcal{H}_a \otimes \mathcal{H}_F \longrightarrow \mathcal{H}_a \otimes \mathcal{H}_F.$$

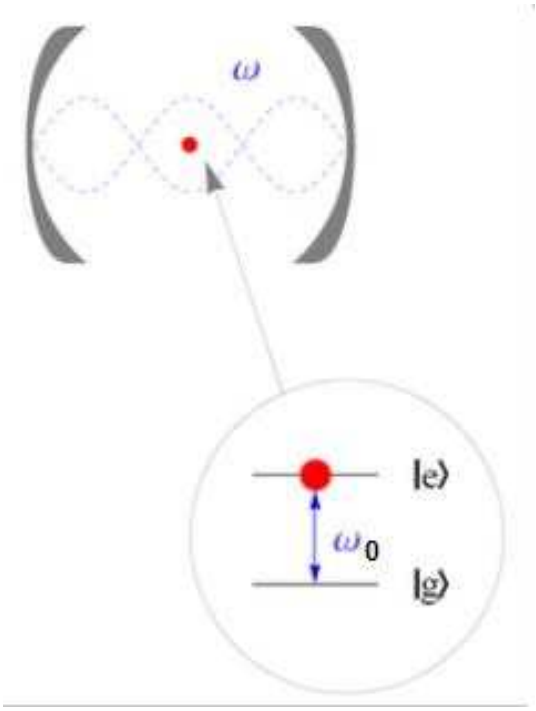

Figure 1.7: Jaynes-Cummings model [7].

The Hilbert spaces $\mathcal{H}_a$ and $\mathcal{H}_F$, as well as the three terms of the Hamiltonian are described below.

H_F describes free EM field in a cavity. It results from a quantization of the EM field with periodic boundary conditions. It turns out that H_F is the *shifted* harmonic

[7] Wikipedia

oscillator[8]

$$H_F = \hbar\omega \hat{a}^* \hat{a} : \quad \mathcal{H}_F \longrightarrow \mathcal{H}_F.$$

The eigenbasis of H_F consists of vectors denoted $|n\rangle$. We have $\mathcal{H}_F = \text{span}\{|n\rangle : n = 0, 1, 2, \ldots\}$. One has

$$\hat{a}\,|n\rangle = \sqrt{n}\,|n-1\rangle$$

and

$$\hat{a}^*\,|n\rangle = \sqrt{n+1}\,|n+1\rangle,$$

so that

$$\hat{a}^*\hat{a}\,|n\rangle = n\,|n\rangle.$$

For simplicity, H_a, which describes non-interacting matter, is taken to be a two-level Hamiltonian:

$$H_a = \frac{\hbar\omega_0}{2}(|e\rangle\langle e| - |g\rangle\langle g|) : \quad \mathcal{H}_a \longrightarrow \mathcal{H}_a,$$

where $\mathcal{H}_a = \text{span}\{|g\rangle, |e\rangle\}$,(This system is called the two-level system). Note that the energy gap between the ground state $|g\rangle$ and the excited state $|e\rangle$ is $\hbar\omega_0$.

Finally, the interaction part H_{int} is defined as

$$H_{int} = \hbar\lambda\,(\sigma_+ \otimes \hat{a} + \sigma_- \otimes \hat{a}^*) : \quad \mathcal{H}_a \otimes \mathcal{H}_F \longrightarrow \mathcal{H}_a \otimes \mathcal{H}_F$$

where

$$\sigma_+ = |e\rangle\langle g| \quad \text{and} \quad \sigma_- = |g\rangle\langle e|.$$

A direct check shows that:

$$(I \otimes H_F + H_a \otimes I + H_{int})\,|g\rangle|n\rangle = (\hbar\omega n - \frac{\hbar\omega_0}{2})\,|g\rangle|n\rangle + \hbar\lambda\sqrt{n}\,|e\rangle|n-1\rangle, \tag{1.4.1}$$

as well as

$$(I \otimes H_F + H_a \otimes I + H_{int})\,|e\rangle|n-1\rangle = (\hbar\omega(n-1) + \frac{\hbar\omega_0}{2})\,|e\rangle|n-1\rangle + \hbar\lambda\sqrt{n}\,|g\rangle|n\rangle, \tag{1.4.2}$$

[8]For computational convenience we take $H_F = \hat{H} - \frac{1}{2}\hbar\omega I$, where $\hat{H}$ is the harmonic oscillator 1.2.1.

Let us represent the composite Hilbert space in the form:

$$\mathcal{H}_a \otimes \mathcal{H}_F \doteq S^0 \oplus \bigoplus_{n=1}^{\infty} S^n,$$

where $S^0 = \text{span}\{|g\rangle|0\rangle\}$, and $S^n = \text{span}\{|g\rangle|n\rangle, |e\rangle|n-1\rangle\}$ for $n = 1, 2, 3, \ldots$.
Following theorem guarantees " $\doteq$".

Theorem 1.4.1. *Suppose A_j's are self-adjoint operators on $\mathcal{H}_j$ then $A = \oplus_j A_j$ is self-adjoint and $R_A(z) = \oplus_j R_{A_j}(z)$, where $z \in \rho(A) = \mathbb{C} \setminus \sigma(A)$ and $\sigma(A) = \overline{\bigcup_j \sigma(A_j)}$ [75].*

Formulas (1.4.1), (1.4.2) show that H filters through this decomposition, i.e.

$$H\,|_{S^n} \colon S^n \longrightarrow S^n, \quad n = 0, 1, 2, \ldots$$

This fundamental property of the Hamiltonian H allows us to understand its properties via a representation of each component as a 2×2 matrix. Let $n > 0$ (the case of $n = 0$ is trivial). In view of (1.4.1), (1.4.2) we can represent $H\,|_{S^n}$ in the basis $\{|g\rangle|n\rangle, |e\rangle|n-1\rangle\}$ as

$$H\,|_{S^n} = \frac{\hbar}{2} \begin{pmatrix} 2\omega n - \omega_0 & 2\lambda\sqrt{n} \\ 2\lambda\sqrt{n} & 2\omega(n-1) + \omega_0 \end{pmatrix}. \tag{1.4.3}$$

Next, we find the eigenvalues $E_\pm(n)$ of $H\,|_{S^n}$. We solve the quadratic equation in ν (defined by $E = \frac{\hbar}{2}\nu$):

$$\det \begin{pmatrix} 2\omega n - \omega_0 - \nu & 2\lambda\sqrt{n} \\ 2\lambda\sqrt{n} & 2\omega(n-1) + \omega_0 - \nu \end{pmatrix} = 0. \tag{1.4.4}$$

It yields

$$\nu = (2n-1)\omega \pm \Omega_n, \quad \text{where } \Omega_n = \left[(\omega - \omega_0)^2 + 4\lambda^2 n\right]^{1/2}$$

The correction term Ω is known as the Rabi frequency. We obtain the following eigenvalues of H:

$$E_\pm(n) = (n - \frac{1}{2})\hbar\omega \pm \frac{\hbar}{2}\Omega_n.$$

Note that in the resonance case $\omega = \omega_0$ the Rabi frequency is $\Omega_n = 2\lambda\sqrt{n}$.

The spectrum of the composite system is different than that of either one of its components. This effect is the main prediction of the Jaynes-Cummings model.

Chapter 2

A Numerically Efficient Approach to The Modelling of Double-Quantum Dot Channels

2.1 Introduction

In the last decade the theory and modelling of quantum dots have attracted a lot of attention and, indeed, the topic may be regarded as one of the central ones in the area of nanotechnology. Researchers have been successful in applying the ab-initio DFT simulation to explain the fundamental characteristics of a single quantum dot, which is typically considered as an artificial molecule, see e.g. [52], [53]. More recently there has been a lot of enthusiasm about nano-systems that consist of a pair of interacting quantum dots, here referred to as the double-Qdots. One of the remarkable examples is a double-Qdot comprising two *single-electron* quantum dots, see [61] and also [21]. Since these double-Qdots provide a means for controlling the electron spin via gate potentials—effectively implementing a spin-swap which is a fundamental quantum computing operation, [48]—they may well become the enabling hardware components of a quantum computer. Some very significant progress toward developing addressable quantum registers based on this type of technology was reported in [15]. A very promising feature of these new structures is their comparatively long coherence time. Of course, apart from quantum computing, the double-Qdots are bound to find other electronic applications, e.g. substituting for the traditional piezoelectric sensors, [45].

In light of this it is vital to develop good models for the electronic structure of double-Qdot systems and, indeed, the topic attracts a lot of attention. Of note are the early *ab initio* models, [69] or [81]. In addition, there has been progress in the modelling of a double-Qdot with metal contacts via the Non-equilibrium Green's Function Theory (NEGF). In particular, in [48] the authors assessed the validity of the equation of motion approach to the NEGF formalism specifically for a double-Qdot coupled with two contacts. The model takes into account both intra- and intro-dot Coulomb interactions. In general, the equation of motion NEGF formalism provides a qualitative description of transport phenomena that occur in strongly correlated systems, such as the Coulomb blockade effect and the Kondo effect. The authors study the effect of different approximate closures to the equation of motion NEGF formalism on steady state properties within an extended Hubbard model (also known as the double Anderson model). For comparison in [74] the authors consider a NEGF model based on a Hubbard type Hamiltonian, which accounts for tunneling type electron transfer between the two Qdots as well as the isolator-type electrostatic Coulomb interaction between them. The effect of contacts is also modelled via a tunneling electron transport. Yet another approach is taken in [39] wherein the electron transport, in structures such as the Qdots or single molecules, is captured via a quantum master equation. Naturally, this is meant as a brief introductory outline. While a complete literature review would go beyond the scope of this chapter, we return to the topic of NEGF and consider some additional aspects of this theory in Section 2.7.

It is vital to realize that a typical model of a double-Qdot system, be it of the *ab initio* or the NEGF type requires intensive computation. At the same time some applications of modelling—such as, say, production quality control, but also numerical experimentation for the sake of fundamental research—require high numerical efficiency ensuring real time computability. In this chapter we undertake to consider a new class of models for double-Qdots, which enable some scalability of computational complexity. The proposed composite-quantum-system type model is to the author best knowledge conceptually novel and hitherto unexplored. It is based on a Hamiltonian for a bipartite quantum

system, wherein the subsystem Hamiltonians are given *a priori*, and the interaction term is constructed with the use of a convolution or a Wiener-Hopf type operator, see e.g. [10], [47]. Our decision to focus on this type of interaction term arose from a dictum that if a new mathematical structure is to be constructed to capture the essence of an element of increased complexity, it is probably best done with as much conceptual parsimony and as few additional "ingredients" as possible. Indeed, the proposed model is perhaps the simplest possible, given that it must incorporate each single Qdot's dynamics and needs to account for the Qdot-Qdot interaction. We emphasize that the interaction is modelled at a rather general level to avoid the complexity trap that would be inevitable in an *ab initio* approach. The type of construction being proposed is perhaps somewhat reminiscent of the classical Jaynes-Cummings model, [40], [70], frequently evoked in Quantum Optics. However, in stark contrast to the Jaynes-Cummings Hamiltonian our model incorporates a high-dimensional parameter (the kernel function) which, by design, can be fitted to a physical system *a posteriori*.

One of the main goals of this chapter is to examine the cumulative density of states function, $N(E)$, arising from the proposed Hamiltonian. We have conducted extensive numerical simulations to understand the dependence of $N(E)$ on the choice of the underlying parameters. As it turns out, the choice of parameters, especially the kernel function, strongly affects the characteristics of $N(E)$, which bodes well for the model's applicability and versatility. We apply the results concerning $N(E)$ to draw conclusions about the electronic characteristics of the double Qdot channel. One of our main findings is summarized in Fig. 2.7. Our model suggests that the functional features of such systems should fall within several distinct categories. In Section 2.6 we give a brief qualitative comparison of these predictions to the known experimental data. In Section 2.7 we discuss a range of issues pertaining to the numerical efficiency of the model at hand.

2.2 Constructing the composite system Hamiltonian

We wish to consider a quantum system that consists of two distinguishable components (subsystems), e.g. two distinct Qdots. We assume that the subsystem properties are well understood and given to us *a priori* as constituents of the model. More specifically, let the dynamic properties of these components, when in isolation, be captured by Hamiltonians $H_i : \mathcal{H}_i \longrightarrow \mathcal{H}_i$ $(i = 1, 2)$, both having pure-point spectrum. In order to fix notation let us specify the eigenstates:

$$H_1(\psi_k) = E_k\,\psi_k, \qquad \text{and} \qquad H_2(\phi_l) = F_l\,\phi_l,$$

where, for convenience, we allow the eigenstates to be indexed by arbitrary integers, i.e. $k, l \in \mathbb{Z}$. Note that the two bases — i.e. $\{\psi_k\}_{k\in\mathbb{Z}}$ and $\{\phi_l\}_{k\in\mathbb{Z}}$ — furnish the Hilbert space isomorphisms $\mathcal{H}_i \cong \ell_2(\mathbb{Z})$ $(i = 1, 2.)$

Next, construct the composite system Hamiltonian $H : \mathcal{H}_1 \otimes \mathcal{H}_2 \longrightarrow \mathcal{H}_1 \otimes \mathcal{H}_2$ in the form

$$H = H_1 \otimes I + I \otimes H_2 + \lambda H_{int}, \tag{2.2.1}$$

which accounts for inter-component interaction. We wish to propose a simple model for H_{int}. First, observe that the basis $\{\psi_k \otimes \phi_l\}_{(k,l)\in\mathbb{Z}^2}$ furnishes an identification $\mathcal{H}_1 \otimes \mathcal{H}_2 \cong \ell_2(\mathbb{Z}) \otimes \ell_2(\mathbb{Z}) \cong \ell_2(\mathbb{Z}^2)$ via a unitary map T:

$$T : \mathcal{H}_1 \otimes \mathcal{H}_2 \longrightarrow \ell_2(\mathbb{Z}^2)$$

$$|\psi_k\rangle|\phi_l\rangle \longmapsto \delta_{(k,l)}.$$

In other words, for a composite system state vector $\Psi \in \mathcal{H}_1 \otimes \mathcal{H}_2$ we obtain $T\Psi = X \in \ell_2(\mathbb{Z}^2)$, such that

$$\Psi = \sum_{(k,l)\in\mathbb{Z}^2} X(k,l)\,|\psi_k\rangle|\phi_l\rangle \quad (\text{notation: } |\psi_k\rangle|\phi_l\rangle = \psi_k \otimes \phi_l). \tag{2.2.2}$$

Second, consider a matrix $K \in \ell_2(\mathbb{Z}^2)$ (whose properties will be specified later). We attempt to prescribe the interaction Hamiltonian by

$$H_{int}\Psi = \sum_{(k,l)\in\mathbb{Z}^2} Y(k,l)\,|\psi_k\rangle|\phi_l\rangle,$$

where

$$Y = K * X, \qquad \text{i.e.} \qquad Y(n_1, n_2) = \sum_{(k,l)\in\mathbb{Z}^2} K(n_1 - k, n_2 - l)\, X(k, l).$$

In other words,

$$H_{int}\Psi = T^* K * T\Psi \qquad \text{equivalently} \qquad T H_{int} T^* = K * . \tag{2.2.3}$$

Of course, we need to specify conditions on K for H_{int} to be a viable interaction Hamiltonian. The first issue of concern is ensuring self-adjointness $H_{int}^* = H_{int}$. In order to resolve the problem we proceed as follows. Let us define a unitary operator

$$\mathcal{U} : \mathcal{H}_1 \otimes \mathcal{H}_2 \longrightarrow L_2([0, 2\pi]^2)$$

$$|\psi_k\rangle|\phi_l\rangle \longmapsto e^{ikx} e^{ily},$$

and let $\mathcal{F}$ denote the unitary map of the Fourier transform, i.e.

$$\mathcal{F} : L_2([0, 2\pi]^2) \longrightarrow \ell_2(\mathbb{Z}^2),$$

$$e^{ikx} e^{ily} \longmapsto \delta_{(k,l)}.$$

We can summarize above discussion in following diagram

$$\begin{array}{ccc} \mathcal{H}_1 \otimes \mathcal{H}_2 & \xrightarrow{\quad \mathcal{U} \quad} & L_2([0, 2\pi]^2) \\ \Big\downarrow{\scriptstyle T} & & \Big\uparrow{\scriptstyle id} \\ \ell_2(\mathbb{Z}^2) & \xrightarrow{\quad \mathcal{F}^* \quad} & L_2([0, 2\pi]^2) \end{array}$$

We write $\mathcal{F}X = \check{X}$. As is well known the Fourier transform is an algebra homomorphism which trades multiplication for convolution. Therefore, $K * X = \mathcal{F}(\check{K} \cdot \check{X})$. Let $V = \check{K} \in L_2([0, 2\pi]^2)$, and let $V_\times : L_2([0, 2\pi]^2) \to L_2([0, 2\pi]^2)$ denote the operator of multiplication by V. By (2.2.3) we have $T H_{int} T^* = \mathcal{F} V_\times \mathcal{F}^*$ or, equivalently,

$$H_{int} = T^* \mathcal{F} V_\times \mathcal{F}^* T = \mathcal{U}^* V_\times \mathcal{U}. \tag{2.2.4}$$

It is now clear that H_{int} is formally self-adjoint iff $V = \check{K}$ is real valued. This observation is also helpful in describing the analytic properties of H_{int}, although we do not undertake to do so in this chapter, which is focused on numerical experimentation.

Remark 2.2.1. In the special case of $H_1 = \frac{d^2}{dx^2}$, $H_2 = \frac{d^2}{dy^2}$, with (x, y) in the flat torus, the unitary operator $\mathcal{U}$ in (2.2.4) is in fact an identity, and so H given by (2.2.1) is in fact equivalent to the Schrödinger operator with the potential $V = \check{K} \in L_2([0, 2\pi]^2)$. In light of this (2.2.1) may be viewed as a generalization of the standard Schrödinger model.

2.3 Examining the special case

For the Hamiltonian H with the convolution kernel $K = \delta_{(1,-1)} + \delta_{(-1,1)}$, one obtains

$$H_{int}|\varphi_k\rangle|\psi_l\rangle = |\varphi_{k-1}\rangle|\psi_{l+1}\rangle + |\varphi_{k+1}\rangle|\psi_{l-1}\rangle.$$

Furthermore, let us fix the subsystem Hamiltonians H_1, H_2 with equal discrete energy spectra $E_n = F_n$ and $E_n = 0$ for $n \leqslant 0$. Departing slightly from convolution scenario, we consider the Hamiltonian $\bar{H} = P \circ H$ where $P : \ell_2(\mathbb{Z}^2) \longrightarrow \ell_2(\mathbb{Z}^2_+)$ is the projection operator. This construction closely resembles the architecture of the classical Wiener-Hopf operators. We are going to represent the composite system Hamiltonian in the basis $\{|\varphi_k\rangle|\psi_l\rangle\}$ ordered in a special way as follows:

$$\begin{aligned}
&|\varphi_0\rangle|\psi_0\rangle, && (k+l=0)\\
&|\varphi_1\rangle|\psi_0\rangle,\ |\varphi_0\rangle|\psi_1\rangle, && (k+l=1)\\
&|\varphi_2\rangle|\psi_0\rangle,\ |\varphi_1\rangle|\psi_1\rangle,\ |\varphi_0\rangle|\psi_2\rangle, && (k+l=2)\\
&|\varphi_3\rangle|\psi_0\rangle,\ |\varphi_2\rangle|\psi_1\rangle,\ |\varphi_1\rangle|\psi_2\rangle,\ |\varphi_0\rangle|\psi_3\rangle, && (k+l=3)\\
&\vdots
\end{aligned}$$

Observe

$$\bar{H}\,|\varphi_2\rangle|\psi_0\rangle = (E_2 + E_0)\,|\varphi_2\rangle|\psi_0\rangle + \lambda\,|\varphi_1\rangle|\psi_1\rangle,$$
$$\bar{H}\,|\varphi_1\rangle|\psi_1\rangle = (E_1 + E_1)\,|\varphi_1\rangle|\psi_1\rangle + \lambda\,|\varphi_0\rangle|\psi_2\rangle + \lambda\,|\varphi_2\rangle|\psi_0\rangle,$$
$$\bar{H}\,|\varphi_0\rangle|\psi_2\rangle = (E_0 + E_2)\,|\varphi_0\rangle|\psi_2\rangle + \lambda\,|\varphi_1\rangle|\psi_1\rangle, \ \ldots \text{ etc.}$$

Thus $\bar{H}$ is represented by the following block structured matrix:

$$\bar{H} = \begin{pmatrix} E_0+E_0 & 0 & 0 & 0 & 0 & 0 & \cdots & \cdots \\ 0 & E_1+E_0 & \lambda & 0 & 0 & 0 & \cdots & \cdots \\ 0 & \lambda & E_0+E_1 & 0 & 0 & 0 & \cdots & \cdots \\ 0 & 0 & 0 & E_2+E_0 & \lambda & 0 & \cdots & \cdots \\ 0 & 0 & 0 & \lambda & E_1+E_1 & \lambda & \cdots & \cdots \\ 0 & 0 & 0 & 0 & \lambda & E_0+E_2 & \cdots & \cdots \\ \vdots & \vdots & \vdots & \vdots & \vdots & \vdots & \ddots & \vdots \end{pmatrix}$$

When the energy levels are those of a harmonic oscillator[1], i.e. $E_n = \frac{2n+1}{2}$, the H matrix consists of increasing diagonal blocks of the form:

$$H_N = \begin{pmatrix} N & \lambda & 0 & \cdots & 0 & 0 \\ \lambda & N & \lambda & \cdots & 0 & 0 \\ 0 & \lambda & N & \cdots & 0 & 0 \\ \vdots & \vdots & \vdots & \ddots & \lambda & 0 \\ 0 & 0 & 0 & \cdots & N & \lambda \\ 0 & 0 & 0 & \cdots & \lambda & N \end{pmatrix}$$

The eigenvalues of such matrices may be calculated explicitly by using the row expansion of the determinant that results in a recurrence relation. Characteristic polynomial of H_n is:

$$\begin{aligned} C_N(x) &= det(H_N - xI_N) \\ &= det \begin{pmatrix} N-x & \lambda & 0 & \cdots & 0 & 0 \\ \lambda & N-x & \lambda & \cdots & 0 & 0 \\ 0 & \lambda & N-x & \cdots & 0 & 0 \\ \vdots & \vdots & \vdots & \ddots & \vdots & 0 \\ 0 & 0 & 0 & \cdots & N-x & \lambda \\ 0 & 0 & 0 & \cdots & \lambda & N-x \end{pmatrix} \end{aligned}$$

[1]Since the model is parametric by design and all the essential predictions are of qualitative nature, the physical constants may be viewed as parameters and are here set at trivial values for convenience.

In order to calculate eigenvalues of $C_N(x)$, we state with observation that

$$C_N(x) = (N-x)C_{N-1}(x) - \lambda^2 C_{N-2}(x), \tag{2.3.1}$$

where $C_{N-1}(x)$ obtained from $C_N(x)$ by omitting the first row and the first column.

In order to solve above recurrence equation we apply the following well-known lemma

Lemma 2.3.1. *If $x_1 = 1$ and $x_2 = A$ the general solution of second order linear recurrence equation $x_N = Ax_{N-1} + Bx_{N-2}$ is $x_N = \frac{a^N - b^N}{a-b}$ where a and b are solutions of $x^2 - Ax - B = 0$.*

The lemma is easily seen to be hold true by means of an application of Vieta's formulas.

In our case, $A = (N-x)$ and $B = -\lambda^2$, so $a = \frac{1}{2}((N-x) + \sqrt{(N-x)^2 - 4\lambda^2})$ and $b = \frac{1}{2}((N-x) - \sqrt{(N-x)^2 - 4\lambda^2})$.

Assume

$$\Delta_N = \frac{a^{N+1} - b^{N+1}}{a-b}.$$

Easily one can observe that

$$\Delta_N = A\Delta_{N-1} - \lambda^2 \Delta_{N-2}$$

Thus, according to equation 2.3.1

$$C_N(x) = \frac{a^{N+1} - b^{N+1}}{\sqrt{(N-x)^2 - 4\lambda^2}}.$$

Next, assuming $C_N(x) = 0$ we obtain $a^{N+1} = b^{N+1}$, or equivalently

$$((N-x) + \sqrt{(N-x)^2 - 4\lambda^2})^{N+1} = ((N-x) - \sqrt{(N-x)^2 - 4\lambda^2})^{N+1}$$

substituting $z = (N-x)$ we get

$$(z + \sqrt{z^2 - 4\lambda^2})^{N+1} = (z - \sqrt{z^2 - 4\lambda^2})^{N+1}$$

i.e. $(\frac{z+\sqrt{z^2-4\lambda^2}}{z-\sqrt{z^2-4\lambda^2}})^{N+1} = 1$. Multiplying the numerator and the denominator by the congruent of the denominator yields $(\frac{(z+\sqrt{z^2-4\lambda})}{2\lambda})^{2(N+1)} = 1$, hence

$$\frac{(z+\sqrt{z^2-4\lambda})}{2\lambda} = e^{\frac{2k\pi i}{2(N+1)}}, k = 1, 2, \cdots, 2N+1.$$

The last equation yields $z = \lambda\frac{1+e^{\frac{2k\pi i}{N+1}}}{e^{\frac{k\pi i}{N+1}}}$. Multiplying the numerator and the denominator of the fraction by $e^{-\frac{k\pi i}{N+1}}$ we get $z = 2\lambda cos(\frac{k\pi}{N+1})$, in summary, the eigenvalues turn out to be:

$$E_{N,k} = N - 2\lambda \cos\frac{k\pi}{N+1},\ k = 1, \ldots, N. \tag{2.3.2}$$

The doubly-indexed collection $\{E_{N,k} : k = 1, \ldots, N,\ N = 1, 2, 3, \ldots\}$ is the complete set of the eigenvalues of the H matrix. Another method for calculating the eigenvalues of H_N can be found in[11].

We have used the above observation to test the correctness as well as the accuracy of the general numerical experiments with the Hamiltonian (2.2.1)-(2.2.3). In order to briefly summarize our findings, let $\{e_i : i = 1, 2, 3, \ldots, N(N+1)/2\}$ be the complete set of *theoretical* eigenvalues of $\bar{H}$, i.e. the eigenvalues are determined via formula (2.3.2) and ordered according to their magnitudes. Similarly, let $\{\mathcal{E}_i : i = 1, 2, 3, \ldots, N(N+1)/2\}$ denote the magnitude-ordered eigenvalues of H resulting from *numerical simulation*. The maximal distance $|e_i - \mathcal{E}_i|$ may then be regarded as a measure of accuracy of the numerical schema used to obtain $\{\mathcal{E}_i\}$. In this way we have established convincing evidence for the reliability of our specific numerical schema, which is described in the Appendix. To give an example, we find that for $N = 21$ and $\lambda = 1$ or $\lambda = 10$, $\max\{|\ e_i - \mathcal{E}_i\ | : i = 1, 2, 3, \ldots, N(N+1)/2\} \cong 10^{-14}$ and for $\lambda = 100$ the accuracy is hardly diminished at 10^{-13}.

2.4 Modelling a double-Qdot channel

We wish to consider a conceptual semiconductor channel device comprising two (similar or identical) quantum dots suspended in between metal contacts (source and drain), see Fig. 2.1. In a laboratory setting the Qdots become coupled when brought into physical proximity, close enough for the electron clouds to interleave. It is intuitively natural to expect that within a moderate range of the inter-Qdot distances the qualitative nature

of the interaction remains unchanged, while its strength should depend on the actual distance, e.g. it might be in the inverse proportion to it. Note that the difference between a nanoscopic system such as the one at hand and a microscopic one is that it precludes the possibility of chemical bonding. We believe that systems as these may find numerous applications in electronics and sensing, including the problem of detecting and quantifying the strength of micro-vibrations. In light of this, we find it interesting to understand the dependence of their *strength of interaction-to-conductivity* characteristic on the parameters characterizing a given set of components and their geometry. This is the focus of the remainder of this chapter.

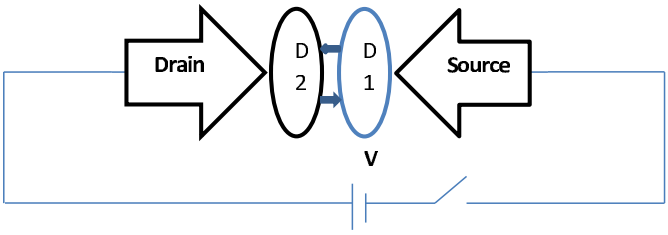

Figure 2.1: The simplest circuit with the double Qdot channel (DQDC).

In order to come up with a workable conceptual model of the system at hand, we will ignore the effect of the contact-Qdot interaction (— for additional comments see Remarks at the end of this section), and focus solely on the double Qdot subsystem. Subsequently, we elect to view the double Qdot as a bipartite quantum system, and construct its model via Hamiltonians of type (2.2.1)-(2.2.3), experimenting with different choices of the constituent parameters, including several deliberate modifications of the kernel function K. The role of the kernel is to capture, at least qualitatively, the inter-Qdot interaction, while the parameter λ moderates its strength. In light of the proposed interpretation λ may be conceived of as a parameter quantifying the effect of the adjustment of the inter-Qdot distance.

Another external parameter is the number of electrons, which we fix throughout the discussion, assuming that each of the Qdots has $2N$ orbital electrons. Furthermore, we ignore the effect of temperature, e.g. when the Qdots are in isolation, the electrons occupy the first N of the energy levels determined by H_1 and H_2 respectively, i.e. two

opposite spin electrons per level. For simplicity, we assume that $H_1 = H_2$ are the harmonic oscillators.

At equilibrium, the system has a common Fermi energy E_F which is equal to the electrochemical potentials of source μ_s and drain μ_d. On the other hand, when voltage V is applied across the double-Qdot channel, the two electrochemical potential levels split ($\mu_s - \mu_d = qV$). If $\mu_s > E_F \geq \mu_d$, with μ_s sufficiently high, there exist unoccupied levels of energy in the molecule within the range $[\mu_d, \mu_s]$. In these conditions a current is forced through the double Qdot channel, see the schematic representation in Fig. 2.2. The electric charge is transported in charge quanta of $-1e$ by electrons.

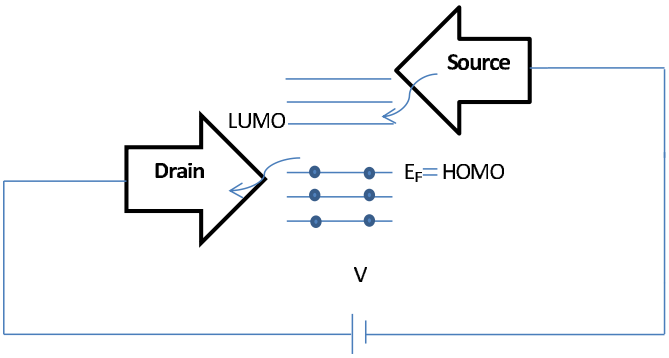

Figure 2.2: Schematic representation of the concepts used to determine the conductivity of the DQDC. Note that the Fermi energy E_F exactly coincides with the HOMO level (at zero temperature).

We discuss the problem of calculating the conductivity of a double Qdot channel placed between the source and drain contacts (DQDC for short). To this end, we invoke *the density of states* function $D(E)$, and the *cumulative density of states* function $N(E)$. Denoting $\mathcal{E}_i$ the eigenvalues of the composite system Hamiltonian H, we have

$$D(E) = \sum_i \delta(E - \mathcal{E}_i),$$

and

$$N(E) = \int_{-\infty}^{E} D(E)dE.$$

Briefly, since $D(E)$ is a string of delta functions, $N(E)$ is the counting function which increases in steps of size one as the variable E passes through each energy level.

As mentioned above, the first assumption is that the DQDC is a quantum system whose dynamics is governed by the Hamiltonian H of the type (2.2.1)-(2.2.3). Secondly, we assume that the conductivity $\kappa(E)$ of the DQDC per spectral range dE is proportional to the number of energy levels in $[E, E + dE]$. More precisely, we have $\kappa(E) = kD(E)$, where the coefficient of proportionality k depends on a variety of external parameters such as the effective electron mass, the mean free time, and the geometry of the system, [18]. Thus, assuming for simplicity $\mu_d = 0$, $\mu_s = qV$, the overall conductivity is the sum of $\kappa(E)$ over the span of unoccupied energy levels below the applied potential:

$$\kappa = \int_{E_F}^{V} \kappa(E)\, dE = k\left[N(V) - N(E_F)\right]. \tag{2.4.1}$$

This formula is the foundation for the numerical study of the conductivity properties of a DQDC in the next section.

Remarks. In applications a DQDC element is typically hooked up to a circuit via a pair of contacts (metal leads). While the discussion of DQDC carried out above abstracts from the effects induced by the contacts, the conductivity of the device as a whole could still be modelled via an effective Hamiltonian. However, in some applications it is of interest to separate the effect of contacts and make it an inherent part of the model. As mentioned in the Introduction such effects are typically modelled within the framework of the NEGF (also known as the Keldysh calculus)[2]. Following [59] we observe that at the phenomenological level the main effect of coupling to the contacts is *energy level broadening* as well as a *shift of the effective Fermi energy level*. The energy level broadening induces flow of a fractional-charge current through the DQDC, even if there are effectively no "pure energy levels" in the interval $[\mu_d, \mu_s]$. Also, the Fermi energy level is effectively shifted to occupy a position mediating between HOMO and LUMO, whose exact value is typically left free as an adjustable parameter that may be fitted to

[2]A similar approach was taken early on in a study of the conductivity of a molecule suspended between two metal leads, [59].

a system *a posteriori*. (Note that if charge transport is effected in integer quanta, the Fermi energy coincides with the HOMO level, as schematically indicated in Fig. 2.2.) A slew of additional corrections would originate from lifting the assumption of absolute-zero temperature (leading to a different statistics of energy-level occupation). At the end of Section 2.7 we briefly discuss the consequences for numerical efficiency that stem from extending the model to explicitly account for the coupling to contacts.

2.5 Numerical Experiments

We report the results of a numerical study of the λ-to-κ characteristic of a DQDC with different choices of the kernel function K. Recall that we base the model of a DQDC on a Hamiltonian of type (2.2.1)-(2.2.3), and calculate the across-channel conductivity via formula (2.4.1). Another of the underlying *a priori* assumptions is the number of occupied levels, i.e. the number of orbital electrons. We have developed numerical algorithms in the MATLAB environment. At this stage, the real-time experimentation is feasible only for relatively small numbers of orbital electrons. Nevertheless, we believe these results outline a qualitatively adequate picture. Our main findings are presented in Figures (2.3)-(2.6). The graphs illustrate the dependence of $N(E)$ on K. We have used the following two kernel types:

1. The "special" K is as in Section 2.3.

2. The "periodic" K is a kernel matrix built in two steps: First, take a matrix L whose rows are filled with the values of a discretized periodic function, e.g. sin. Second, take K to be the Fourier transformed L.

It is interesting to observe that regardless of the kernel the graphs tend to be characterized by stronger concavity of their course scale shape for smaller values of λ.

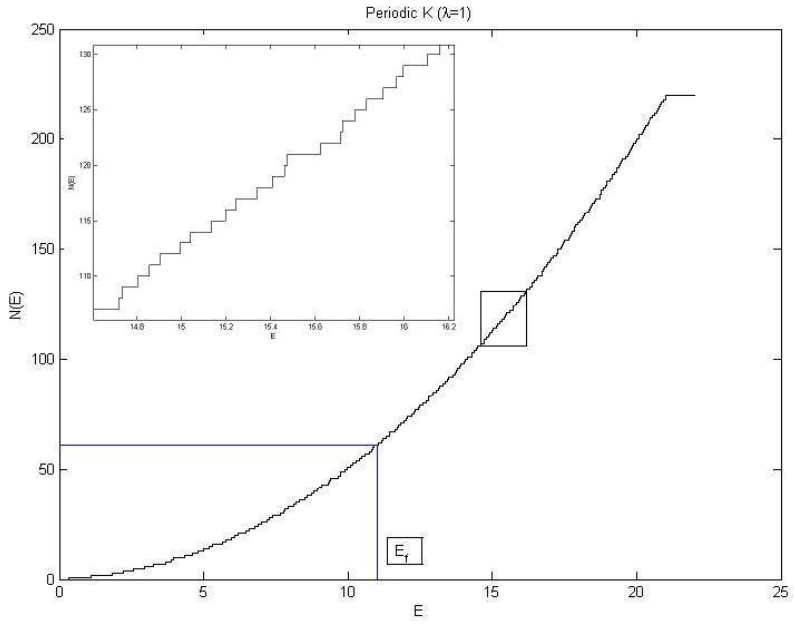

Figure 2.3: The cumulative density of states function $N(E)$ for the periodic K and coupling constant $\lambda = 1$.

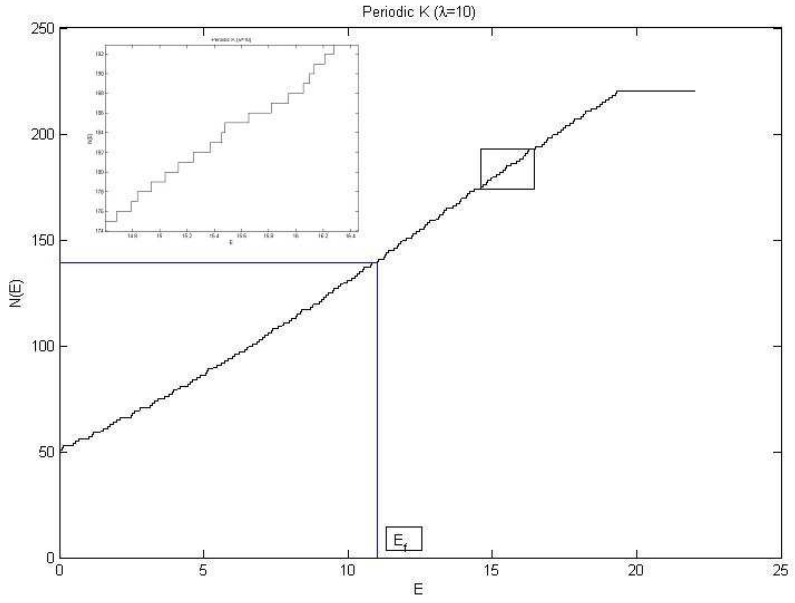

Figure 2.4: The cumulative density of states function $N(E)$ for the periodic K and coupling constant $\lambda = 10$.

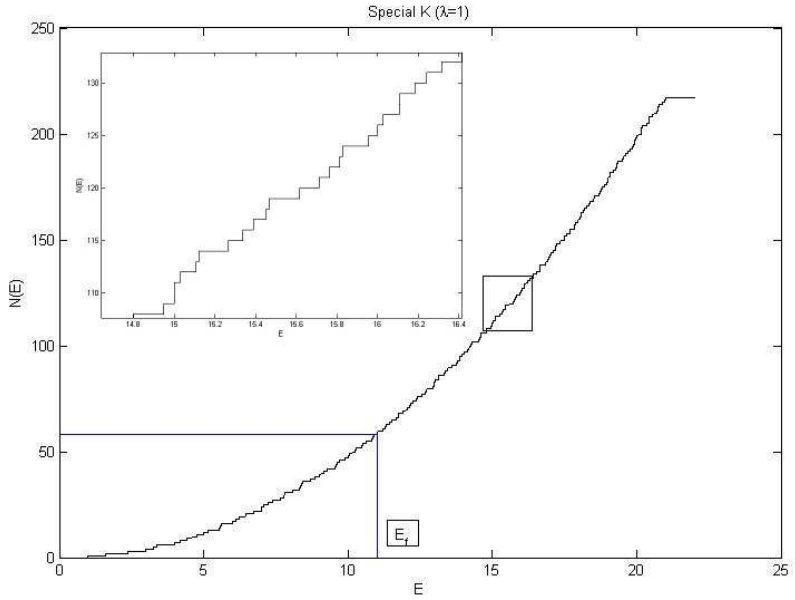

Figure 2.5: The cumulative density of states function $N(E)$ for the special K and coupling constant $\lambda = 1$.

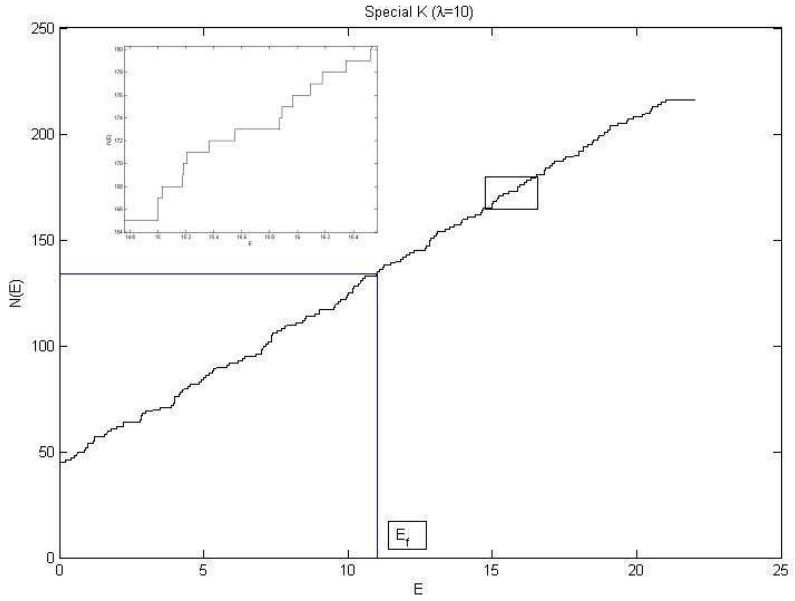

Figure 2.6: The cumulative density of states function $N(E)$ for the special K and coupling constant $\lambda = 10$.

Fig. 2.7 displays the dependence of DQDC's conductivity κ on the coupling constant λ for three different Ks. In addition to the two kernel types described above, we have also considered a random type kernel, i.e. a kernel obtained via the discrete Fourier transform of a random matrix[3]. Clearly the three λ-to-κ curves display individualized and significantly differentiated characteristics, which evidences the proposed model's versatility. We predict all the three λ-to-κ profiles and possibly more to be physically realizable. We also expect the model to be broadly adaptable to the analysis of other systems with bi-partite architectures.

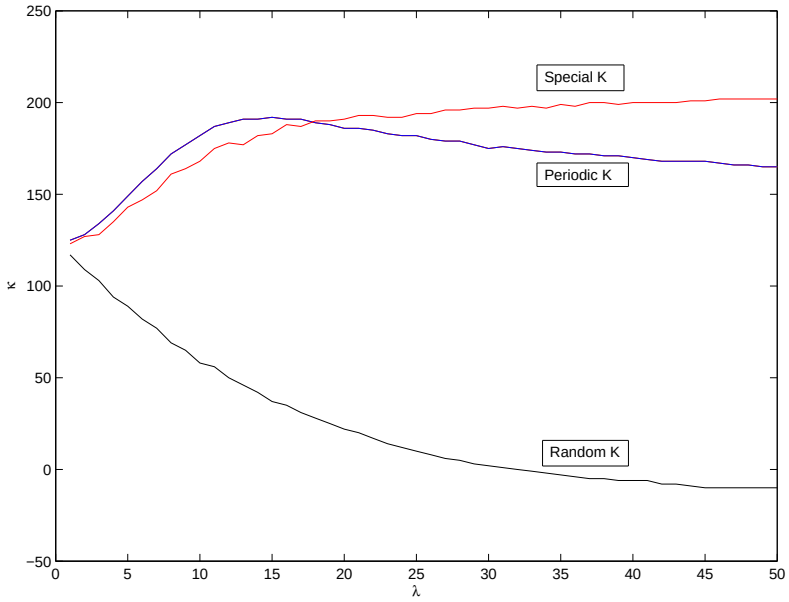

Figure 2.7: Conductivity κ of a double-Qdot channel (DQDC) as a function of the coupling constant λ for three different kernel functions. For computational efficiency the number of orbital electrons has been fixed at a low value (21).

Remark. An additional, finer characterization of the properties of the model at hand depends on the statistical profile of the fine-scale oscillations found in the $N(E)$ curves

[3]Here, a *random matrix* means a matrix populated by uniformly distributed (in $[0,1]$) random numbers obtained with one of the MATLAB's standard random number generators.

(—see box inserts in Figs. 2.3-2.6). We anticipate further results in this direction which will be reported in the next chapter.

2.6 Qualitative comparison to the experimental data

Several experimental studies of the DQDC type structures may be found in the literature, e.g. [41]. In particular, the aforementioned article [15] reports, among other results, conductivity measurements of a particular DQDC structure, referred to as the single electron transistor (SET). The electronic characteristic of a SET is controlled by a pair of gate potentials (V_{G1}, V_{G2}). Clearly, the gate potentials adjust the electrochemical potentials of the two QDots. However, their overall influence on the structure and function of a SET is more complex than that as even the fundamental Hamiltonian is profoundly affected by these parameters.

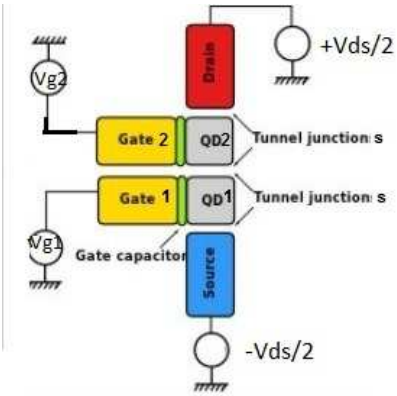

Figure 2.8: Schematic structure of a SET with DQD.

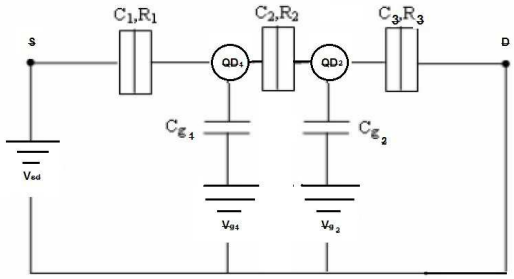

Figure 2.9: Single electron transistor circuits with DQD.

Indeed, the external electric field modifies the shape of the electronic wave function and through that influences Coulomb interactions as well as the hyperfine coupling between the electron and nuclear spins. The reported measurement of source-drain current at a constant applied source-drain bias, see Fig. 1f-g therein, demonstrates strong dependence of conductivity on (V_{G1}, V_{G2}). One of the striking features is the presence of abrupt, nearly discontinuous, changes in conductivity as (V_{G1}, V_{G2}) traverses different regions of the plane. This particular result may be reinterpreted within the framework proposed here. Indeed, we postulate that the two-dimensional (V_{G1}, V_{G2})–space can be mapped into our model's high-dimensional (λ, K)–space in such way as to carry over the essential features of the effective Hamiltonian. Note that due to inherent complexity the exact dependence of the Hamiltonian on the gate potentials is unknown. Nevertheless, there are strong similarities between our predictions and the reported experimental findings. Indeed, our simulations demonstrate that continuous change in λ effects continuous adjustment of the conductivity, whereas qualitative change in K effects conductivity jumps, Fig. 2.7. In light of that it should be possible, at least in principle, to find a translation rule $(\lambda, K) = \Phi[V_{G1}, V_{G2}]$[4] resulting in the accurate predicted conductivity function. Such a task might be attempted via the known techniques for automated parameter fitting.

2.7 A discussion of numerical efficiency

In some applications the speed of simulation is the most important parameter. When that is the case it is necessary for the modeller to have the option of easing the simulation accuracy for gains in computational time. This requirement seems to disadvantage simulation schemas based on *ab initio* models, or even higher-level models that rely upon geometrically localized description of the device in question. Indeed, in those cases the only possible speed gains come from relaxing the tolerance of parameter fitting rather than a reduction in the number of parameters itself. Therefore, when speed is of essence there arises a need for models that keep in check the number of tunable parameters, such

[4]Note that Φ could turn out to be a nonlocal functional rather than just a local function.

as the one proposed here.

All simulation that is based on the *fundamental* (as contrasted with the merely *phenomenological*) principles unavoidably involves some computational constants: a computation of the eigenvalues of the matrix representing the Hamiltonian, parameter fitting via optimization algorithms, such as the genetic algorithm or the simulated annealing schema, etc. Given this constraint a speed-up may still be achieved by limiting the complexity of the Hamiltonian matrix. Such a feat may not always be possible, e.g. it is hard to reduce the complexity of a model that relies on the local geometric description of the simulated device. However, one may hope to achieve complexity reduction by delocalization of parameters, which is the approach we have taken.

Let us briefly compare the model proposed here with the one adopted in the highly regarded standard of nano-system simulation, specifically NEMO 3D,[5]. NEMO 3D is a remarkably versatile tool which enables simulation of nano-devices at a rather fundamental level. However, its demand for the computational power is indeed very high, and speed-up can only be achieved via parallel computation with an increased number of nodes. That computational rigidity is at least partly a by-product of the rigidity of the "bottom-up" models that NEMO 3D computation relies upon. Namely, NEMO 3D synthesizes a Hamiltonian of a nano-structure from a description of the global inter-atomic architecture as well as a relatively detailed description of localized atomic orbitals. In order to solve the model it is necessary to compute the eigenvalues of a large matrix whose characteristics are essentially beyond the modeller's control. In particular, this approach offers no possibility of building progressively less complex simplified models for a structure of interest.

In contrast, the model we propose does not incorporate any strictly geometric descriptions of the underlying physical structure. Thus far we observe sufficient flexibility within this framework to simulate fairly complex electronic spectra of structures such as the DQDC, and capture the essential features of their conductivity. Moreover, in the proposed approach there is a possibility of choosing the model complexity within the

[5]Introduction to the NEMO 3D Tool, http://nanohub.org/resources/11080/download/

constraint of desired accuracy of its predictions. In particular, the Hamiltonians may have a block structure by design, offering easy parallellizability. This cannot be achieved with models that relate the Hamiltonian to the local geometric architecture of the device.

In our simulation schema, as in most other, the dominant factor determining the time of computation is the evaluation of the eigenvalues of the Hamiltonian matrix. A computation of the eigenvalues of an $N \times N$ matrix requires $O(N^3)$ arithmetical operations, and becomes prohibitively complex for large N. However, we note that in order to compute conductivity κ, defined in (5), only very selective information about the eigenvalues is used — namely, the number of eigenvalues in the interval $[E_F, V]$. Thus, for this application, the eigenvalues need not be known with high accuracy. Instead, it suffices to localize each eigenvalue inside or outside this interval. While further research is required to fully develop this idea, we expect an increased efficiency of such a computation can be obtained with suitable modifications of iterative schemas such as the celebrated Lanczos iteration, [76].

It is also interesting to briefly consider the changes that would result from extending our model to include an explicit discussion of contacts, particularly the effect it would have on the numerical complexity of the model. In essence the contacts are viewed as a quantum reservoir characterized by a Hamiltonian H_R. The NEGF type coupling of contacts to the central device is expressed via the super-system Hamiltonian

$$\tilde{H} = \begin{pmatrix} H & \tau \\ \tau^* & H_R \end{pmatrix},$$

where the interaction part τ is typically a rectangular sparse matrix. The electronic conductivity through the core is then determined via the effective resolvent (alternatively called the Green's function) $G = G(E)$, which is defined via

$$(E - \tilde{H})^{-1} = \begin{pmatrix} G(E) & G_R(E) \\ G_R(E)^* & G_{RR}(E) \end{pmatrix},$$

While the sub-matrix $G(E)$ is essential, G_R and G_{RR} are merely auxiliary in the construction and play no further role. It is easily seen that $G(E) = [E - H - \Sigma]^{-1}$, where

$\Sigma = \Sigma(E) = \tau[E - H_R]^{-1}\tau^*$. The main observation of the NEGF theory is that the system's conductivity is determined by the quantity Trace$[G\,\Gamma\,G^*]$ with $\Gamma = \sqrt{-1}\,[\Sigma - \Sigma^*]$ in conjunction with the energy level occupation statistics. We observe that the NEGF framework is universal and can be developed for any core Hamiltonian H, including the Hamiltonians proposed here. However, most importantly, the resulting numerical schema involves the inversion of large matrices resulting in a substantially increased demand for the computational power.

2.8 Chapter conclusion

We have analysed the electronic properties of a channel comprising two interacting quantum dots (DQDC) within the framework of a numerically efficient quantum model. The proposed model is based on a bipartite quantum system Hamiltonian with a class of novel convolution or a Wiener-Hopf type interaction term. We have conducted a numerical analysis of the resulting cumulative density of states function and drawn conclusions regarding the dependence of the DQDC's conductivity on the coupling constant. Our results suggest that the proposed model is capable of capturing diverse DQDC characteristics. We consider the nano-structure at hand to be of interest because of its potential significance for next generation sensors and circuits.

Chapter 3

Fine Scale Spectral Analysis

3.1 Introduction

Determining the spectrum of a quantum system as well as its corresponding density of states function are the most important objectives in the study of quantum systems. Despite the fact that we are easily able to calculate the energy levels of a harmonic oscillator or an infinite quantum well it is difficult to calculate the energy levels of most real quantum systems. In the absence of an explicit formula for the energy levels E_n, one might employ approximation methods such as the Bohr-Sommerfeld quantization or the Wentzel-Kramers-Brillouin (WKB) methods, which rely upon the semiclassical approach to quantum mechanics. Semiclassics is a discipline of physics that attempts to compute spectra of a quantum system on the basis of its classical trajectories, adding only two additional ingredients: quantum mechanical superposition principle and the Planck's constant $\hbar$ [8]. The semiclassical method predicts quantum properties, such as energy levels, based on classical trajectories considering quantum phases and the superposition principle. One might be able to drive classical information from a given quantum information such as the spectra and, conversely, one might be able to construct the wave functions and spectra from the classical trajectories and actions of the system. That is the classical-quantum connection.

One of the main questions in this realm is: for a given quantum system, can one determine whether the underlying classical motion is integrable or chaotic? Results con-

cerning the relationship between quantum and classical mechanics can be translated into the language of Differential Geometry. So the previous question can be translated into one of the so-called "drum questions" [43], "Can one hear the chaology of a drum?" In other words, is it possible to decide, only by listening to a drum, whether the rays of elasticity underlying the vibrations of a given drum are chaotic or regular? This is, of course, reminiscent of the famous original question posed by M. Kac [42], "Can one hear the shape of a drum?"

In order to distinguish between integrable and chaotic systems one needs to consider *fluctuations* properties; that is, how the energy levels are distributed around the average density of states $\bar{D}(E) = \frac{d\bar{N}}{dE}$ where

$$\bar{N}(E) = \frac{1}{(2\pi\hbar)^d}\Omega(E),$$

and

$$\Omega(E) = \int\cdots\int_{H(p,q)<E} dq^d dp^d$$

is the volume of energy shell and d is the number of degrees of freedom. Since energy levels corresponding to different systems or different regions of energy levels of the same system may have different *average* density, one must unify average density before comparing fluctuations. To this end one must renormalize the local unit of energy. Such a procedure is called *unfolding.*

The simplest quantity that describes the level fluctuations is the nearest neighbour-hood spacing distribution (NNSD) $p(s)$ where $p(s)ds$ is the probability of finding two adjacent unfolded energy levels in $[s, s+ds]$. For the case of semiclassical regimes the quantum systems whose underlying classical system is integrable, Berry and Tabor [7] show that $p(s)$ is universal and is a exponential distribution

$$p(s) = \exp(-s), \quad 0 \leqslant s < \infty.$$

In their 1984 papers [9], Bohigas, Giannoni and Schmit formulate a conjecture regarding universality of the laws of level fluctuations of a quantum system with an underlying classically chaotic system. The conjecture was derived from a numerical study of the

Sinai billiard. Specifically the conjecture, still unproven, states that:

Spectra of a system whose underlying classical analogue is chaotic has a NNSD as predicted by the Gaussian Orthogonal Ensemble (GOE).

Semiclassical approximation method called the periodic orbit theory is considered to be the main tool with which to prove BGS conjecture. In 1957 Wigner [80] conjectured that the energy levels of a complex nuclear system have similar statistical distribution as the GOE. He proposed the following distribution

$$p(s) \approx \frac{\pi}{2} s \exp(-\frac{\pi}{4} s^2), \quad 0 \leqslant s < \infty.$$

In periodic orbit theory we are able to express the semiclassical density of states as

$$D(E) = \bar{D}(E) + D_{flu}(E).$$

The fluctuating term $D_{flu}(E)$ is given by trace formula introduced by Gutzwiller [34, 35, 36, 37] and by Balian and Bloch [3, 4, 5].

To the best of the author's knowledge the problem of characterizing the universal properties of $p(s)$ in the mixed case, where both chaotic and KAM orbits are present in the phase space, is still unsettled see [57] and references in there.

As mentioned above, certain mathematical tools have been developed to model and understand the fundamental characteristics of atomic nuclei. It remains to be seen if the fundamental characterisation of nano-systems is similar or rather different in some fundamental way. I have embarked on a project to see if the known methodology, including methods for constructing quantum Hamiltonians, may be used to model the fundamental behaviour of nano-systems. In particular I have asked if the spectral properties of objects such as quantum dots are similar or different from those of atomic nuclei. I have applied the apparatus of statistical analysis of spectra, as first developed by the theorists of semiclassical physics, to see whether or not any definitive statements could be made on the comparison between the nano and the nuclear. The main idea that led to the introduction of statistical methods specifically the Random Matrix Theory RMT was the notion of complexity that nowadays is referred to as *chaos* and it is related to the large

number of degrees of freedom involved in a many-body problem. Since nano-systems are many-body systems it is reasonable to expect that the level statistics of such systems are described by RMT or a similar framework.

3.2 A statistical methodology for the analysis of Hamiltonian dynamics

Two important functions of the spectrum of a quantum system are the density of states

$$D(E) = \sum_n \delta(E - E_n).$$

and the spectral staircase function or the cumulative spectral function

$$N(E) = \int_{-\infty}^{E} D(E)dE$$

which gives the number of energy levels E_n with energy less than E.
Differentiating with respect to E yields

$$D(E) = \frac{dN(E)}{dE}.$$

The smooth function $\bar{N}(E)$ corresponding to the function $N(E)$ is the mean staircase function interpolating $N(E)$. Again by differentiating with respect to E we get

$$\bar{D}(E) = \frac{d\bar{N}(E)}{dE}$$

which is called the smooth density of states or average density of states.

We wish to explore statistically the patterns of the spacings between energy levels of a quantum system. To this end we apply the statistical measure which is called the nearest neighbour spacing distribution(NNSD). Suppose we obtain an ordered set of energy levels of a system. Before applying the NNSD method we have to *unfold* the energy levels. The unfolding procedure serves to universalized the system-dependent (non-universal) mean level density $\bar{D}(E)$ [32]. By universality we mean the distribution function of spacings of energy levels will be the same for a broad class of systems [57, 43]. We outline this

universalizing as follows.

Consider two adjacent energy levels $E_n$and E_{n+1} and their difference, the energy level spacing, $S_n = E_{n+1} - E_n$. In order to universalize the distribution function, we replace the spectrum E_n by a new set of numbers e_n with mean spacing 1 [9] defined by

$$e_n = \bar{N}(E_n). \tag{3.2.1}$$

Suppose $s_n = e_{n+1} - e_n$, we are looking for the universal distribution $p(s)$ such that for randomly chosen n, the probability that $s \leqslant s_n \leqslant s + ds$ is $p(s)ds$. In other words the probability of finding pairs (e_n, e_{n+1}) with $e_{n+1} - e_n \in [s, s + ds]$ is $p(s)ds$ [25].

Definition 3.2.1. The nearest neighbour spacing distribution $p(s)$ is the probability that the spacing between two adjacent energy levels is s. It is required that $p(s)$ and its mean satisfy the normalization constraints

$$\int_0^\infty p(s)ds = 1 \quad \int_0^\infty sp(s)ds = 1.$$

The spacing between two adjacent levels in the unfolded spectrum can be obtained by a Taylor series of $\bar{N}(E)$

$$\begin{aligned} e_{n+1} - e_n &= (E_{n+1} - E_n)\frac{d\bar{N}(E_n)}{dE_n} + h.o.t.^{1} \\ &= \frac{E_{n+1} - E_n}{D_n} + h.o.t. \end{aligned} \tag{3.2.2}$$

where $D_n = \frac{1}{\bar{D}(E_n)}$ is the mean level spacing in the vicinity of E_n [1]. Equation (3.2.2) suggests that the direct relation between the original and unfolded spectra is valid when the higher order terms can be neglected, which is expected to happen where the level density is slowly varying [1].

Nuclear physics deals with complicated interacting systems. A quantum system is characterized by its Hamiltonian. Since the Hamiltonian for the nucleus is not known

[1] higher order terms.

RMT was introduced by Wigner in the 1950s [79, 80] and [62] to make statistical inference about nuclei's Hamiltonian and its spectrum particularly the spaces between adjacent energy levels. The method was developed in [22, 23, 24] and [56] to extend its applicability to other systems. In [80] Wigner proposed that the energy level spectra of complicated nuclear systems have statistical properties similar to the spectra of ensembles (collections) of random matrices. This ensemble has to satisfy two statistical conditions on its probability distribution. First, the matrix elements are independent random variables, So the distribution of a matrix is product of the distributions of its under diagonal elements. Second, the probability distribution for the elements of each matrix is invariant with respect to orthogonal transformations of that matrix ($H \longrightarrow O^t H O$.)
It can be shown [80] that these two hypotheses imply Gaussian distributions for elements of each matrix. The variances for these Gaussians are 1 for all the diagonal elements and $\frac{1}{2}$ for all off-diagonal elements.

An excellent approximation to the NNSD for the GOE is given by the *Wigner Surmise*

$$p(s) \approx \frac{\pi}{2} s \exp(-\frac{\pi}{4} s^2), \quad 0 \leqslant s < \infty \tag{3.2.3}$$

introduced by [80] and [62] .
As it turns out the experimental data of nuclear systems fit the Wigner distribution rather well and the predictions of GOE agree approximately, although not exactly [56].
Most of physical systems belong to the category of mixed systems, the motion in some parts of the classical phase space is integrable while it is chaotic in some other parts. Integrable and chaotic systems are the two extremes. Brody generalized the Wigner distribution in order to study mixed systems by means of the Ansatz

$$p(s) = a(1+b)\pi s^b \exp(-a\pi s^{1+b}), \quad a = \frac{1}{\pi}\left(\Gamma(\frac{2+b}{1+b})\right)^{1+b}, \quad 0 \leqslant s < \infty \tag{3.2.4}$$

where b is called a repulsion parameter [12] and [13]. Brody distribution interpolates between two extremes, the exponential distribution ($b = 0$) and the Wigner distribution ($b = 1$).

3.3 Statistical analysis of the double quantum dot model

In Chapter 2 I reported results of a numerical study of the conductivity characteristics of a double quantum dots channel (DQDC) with different choices of the kernel function K. Recall that the model of a DQDC is based on a Hamiltonian of type (2.2.1)-(2.2.3), and a calculation of the across-channel conductivity via formula 2.4.1. Another one of the underlying *a priori* assumptions in that model is the number of occupied levels, i.e. the number of orbital electrons.

In this section, I undertake a deeper analysis of the spectra of the Hamiltonians (2.2.1)-(2.2.3) which probe their statistical characteristics, as well as of the question of their universalized type. The main findings of the model presented in chapter 2 are succinctly encapsulated in the contents of Figs. 3.1 and 3.2. The graphs illustrate the dependence of $N(E)$ on K. We have used the following two kernel types:

1. The "special" $K = \delta_{(1,-1)} + \delta_{(-1,1)}$.

2. The "periodic" K is a kernel matrix built in two steps: First, take a matrix L whose rows are filled with the values of a discretized periodic function, e.g. sin. Second, take K to be the Fourier transformed L.

Although two graphs looks more or less the same on the course scale, they have different finer scale behaviour and structure. In order to study this finer structure we need a new apparatus. The nearest neighbour spacing distribution (NNSD) provides us with a means to study the eigenvalues statistically.

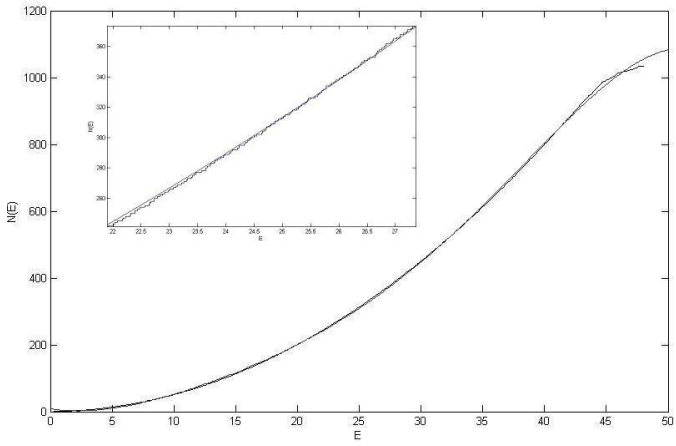

Figure 3.1: $N(E)$ and $\bar{N}(E)$ for the periodic kernels K when $\lambda = 1$ and the number of orbital electrons $N = 45$.

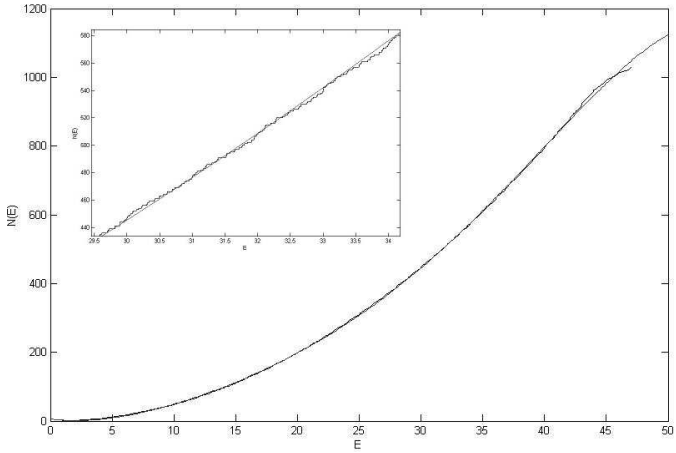

Figure 3.2: $N(E)$ and $\bar{N}(E)$ for the "special" kernels K when $\lambda = 1$ and the number of orbital electrons $N = 45$.

Each one of the above mentioned cases yields a spectrum of the Hamiltonian (2.2.1)-(2.2.3). When the density of states is known, unfolding procedure is possible by employing mean cumulative spectral function $\bar{N}(E)$ to transform the eigenvalues into dimensionless variables with unit mean level spacing. On the other hand, when density of states is not known, as is the case in most practical situations, one usually approximates the

cumulative density of state $N(E)$ by a polynomial [1, 78]. In [1, 78] the authors indicate that the neighbourhood spacing distribution of the spectrum shows little sensitivity to the unfolding method. They indicate as well that the unfolding procedure does not depend strongly on the degree of the polynomial used to interpolate $N(E)$.
In summary, in order to quantify the spectra statistically by employing NNSD. we need to carry out the following steps

1. **Unfolding** In order to unfold spectrum E_n we interpolate $N(E)$ by a polynomial $\bar{N}(E)$ (as mentioned earlier its degree doesn't play a strong role). $e_n = \bar{N}(E)$ is called unfolded spectrum.

2. **Fitting** Fit $\{s_n = e_{n+1} - e_n\}$ to the Brody probability distribution function with an appropriate repulsion parameter.

After step one is carried out for two different kernels, we obtain histograms as follows Figures (3.3) and (3.4).

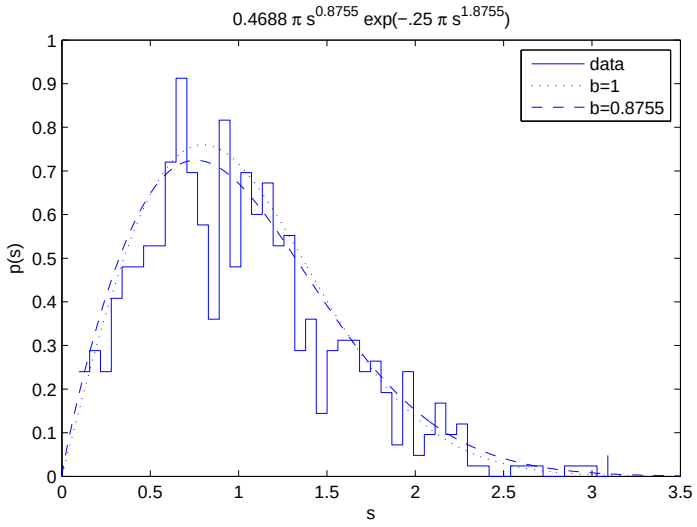

Figure 3.3: NNSD for periodic K, its Brody-type approximation with $b = 0.8755$ and Wigner distribution (b=1).

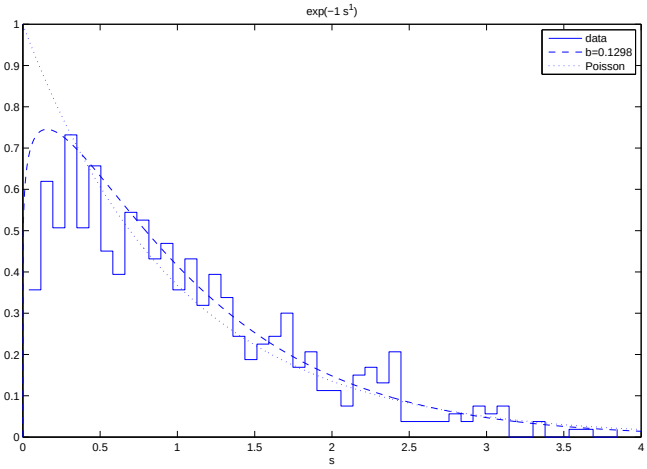

Figure 3.4: NNSD for special K, its Brody-type approximation with $b = 0.1298$ and exponential distribution.

Since the Brody distribution depends on parameter b, first we have to find the best estimator of the parameter (b) for which the distribution will fit the data. There are at least two methods for finding the estimation of the parameter: the method of *maximum likelihood* and the method of *moment estimation*. The latter method is preferable because the former one is cumbersome to solve analytically. However, we obtain confirmation of our results by an application of a standard MATLAB routine which relies upon the second method. Thus, an application of the method of moment estimation yields

$$\frac{1}{n}\sum_{i=1}^{n}(e_i/\bar{e})^2 = \frac{\Gamma(1+\frac{2}{b})}{\Gamma^2(1+\frac{1}{b})}, \tag{3.3.1}$$

where $\bar{e}$ is the mean of the random sample of the unfolded eigenvalues. Solving this equation gives the best estimate for b or the best model and, since $a = \frac{1}{\pi}(\Gamma(\frac{2+b}{1+b}))^{(1+b)}$, one can consequently come up with a .

The particular values we have obtained are as follows. $a = 0.25$ and $b = 0.8755$ for periodic K, and $a = 0.3$ and $b = 0.1298$ for the special K. These outcomes demonstrate that with high likelihood the periodic kernel correspond to a chaotic system and the special kernel a mixed type system.

One of the simplest methods usually employed by statisticians to verify whether a

sample fits a specific distribution or not, is the method of probability plot or quantile-quantile plot, see appendix A. The following Q-Q plots (Figs.3.6 and 3.7) are drawn in order to reinforce the aforementioned outcomes regarding periodic and special kernels respectively. They demonstrate that two distributions with cdfs $F(s) = 1-\exp(-.25\pi s^{1.8755})$ and $F(s) = 1-\exp(-.3\pi s^{1.1298})$ fit the unfolded eigenvalues resulting from the periodic and special kernels respectively.

Figure 3.6 in conjunction with the estimate $b = 0.8755$ which is close to $b = 1$(Wigner distribution) convince us that the periodic kernel yields a Hamiltonian which governs a chaotic system. Figure 3.5 depicts two cases, $b = 0.8755$ and $b = 1$ together. As one observes their behaviour is the same.

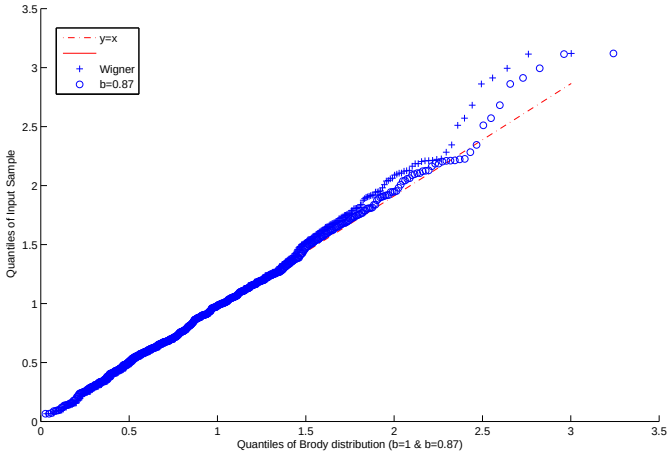

Figure 3.5: Quantiles of Brody distribution for different repulsion parameters vs. quantiles of unfolded eigenvalues corresponding to periodic K.

There are several other statistical methods that can be used to decide if a sample comes from a population with a specific distribution. Some of them are graphical such as the method of quantile-quantile plot and some of them are formal such as the methods of goodness-of-fit. Both have their own advantages and disadvantages. Graphical methods are subjective whereas goodness-of-fit methods are objective. Statisticians usually use the latter methods in order to confirm results of graphical methods, see appendix A. We will follow this tradition, first we us the quantile-quantile plot, see A.1 to demonstrate

that the parameter b which we have found is appropriate.

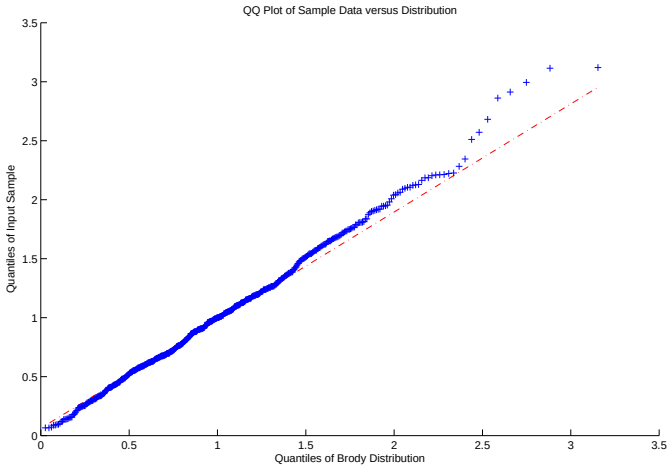

Figure 3.6: Quantiles of Brody distribution for b=0.8755 vs. quantiles of unfolded eigenvalues corresponding to periodic K.

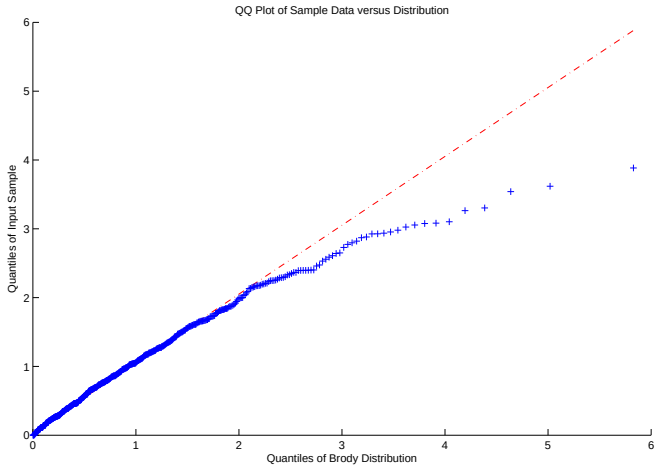

Figure 3.7: Quantiles of Brody distribution for b=0.1298 vs. quantiles of unfolded eigenvalues corresponding to special K.

In order to confirm the above graphical results quantitatively we use Kolmogorov-Smirnov test , see A.2. To this end, we have developed the code, which relies upon the MATLAB “kstest" built-in function to perform Kolmogorov-Smirnov test. Numerical estimates are summarized in the following table.

Kernel(K)	Repulsion parameter(b)
Periodic	$0.62 \leqslant b \leqslant 1$
Special	$0.05 \leqslant b \leqslant 0.42$

Table 3.1: The repulsion parameter b for two different kernels.

Manifestly, the two parameters $b = 0.8755$ and $b = 0.1298$, corresponding to periodic and special kernels respectively, belong to the above mentioned intervals of repulsion parameter b. As one observes, regarding periodic kernel, b can be 1 which corresponds to the Wigner distribution. Since the repulsion parameter at the second row of the table 3.1 can be as small as $b = 0.05$, one might ask, can the unfolded eigenvalues, corresponding to special kernel, be fitted to the exponential distribution $p(s) = e^{-s}$? The following Q-Q plot Fig. 3.8 demonstrates that the answer is negative.

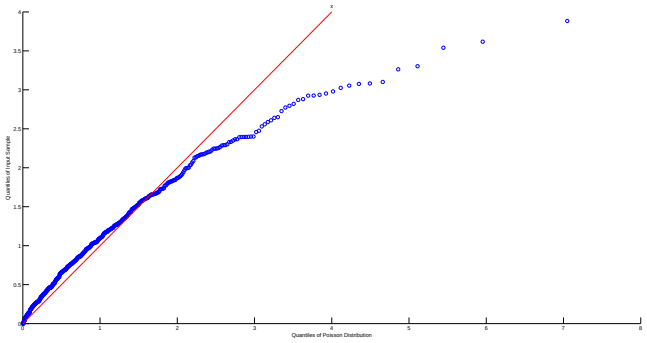

Figure 3.8: Quantiles of exponential distribution vs. quantiles of unfolded eigenvalues corresponding to special K.

This result can be confirmed by the Kolmogorov-Smirnov test as well.

3.4 A comparison with real quantum data

There is a scarcity of real quantum data with quality sufficient to make a meaningful comparison with the proposed model possible. However a notable exception is the data

obtained for the quantum billiard. The quantum billiard has been investigated theoretically [7] as well as numerically [55]. In order to study it experimentally the authors in [31] conducted the following experiment. They considered the quantum billiard corresponding to the Bunimovich stadium which is known to be classically chaotic [7]. The quantum billiard consists of a flat electromagnetic cavity in the shape of a quarter of Bunimovich stadium and approximately flat.

The key point is that the Helmholtz equation, which describes electromagnetic waves in the cavity, is mathematically equivalent to the stationary Schrödinger equation. The outcome of the experiment is the set of about 1060 point spectrum with frequencies between 0.75 and 17.5 GHz. The semiclassical approach is then employed to calculate locations and strengths of the peaks in the Fourier transformed spectrum in terms of classical periodic orbits. The authors also perform a statistical analysis of the spectrum and compare the results to those of the GOE.

We have conducted an analysis of the experimental data analogous to the content of section 3.2. First we approximate the $N(E)$ by $\bar{N}(E)$ in order to unfold the data. To this end the cumulative level density function $N(E)$ versus energy of aforementioned spectrum is drawn and then it is approximated by $\bar{N}(E)$ which fit the data. See figure 3.9. Here $\bar{N}(E)$ is a polynomial of degree three.

Equation 3.2.2 enables us to determine unfolded eigenvalues corresponding to the data. Again, we first try to find the repulsion parameter by the aforementioned statistical methods.

Next, using either the method of moment estimate or the method of maximum likelihood I have been able to find the repulsion parameter b and subsequently the parameter a. Again I use the method of moment estimate and equation 3.3.1 to find a and b similarly as I have done with the periodic and the special kernels. The results are $a = 0.25$ and $b = 0.8376$. Fig. 3.10 shows the NNSD frequency histogram of the 1060 energy levels and its approximation with the Brody distribution with cdf $F(s) = 1 - \exp(-0.25\pi s^{1.8376})$. Note that $b = 0.8376$ is apparently close to the repulsion parameter of the Brody distribution corresponding to the periodic kernel, $b = 0.8755$.

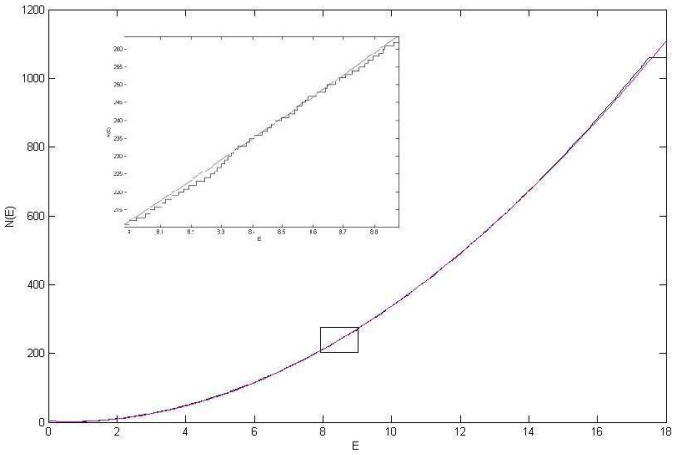

Figure 3.9: $N(E)$ and $\bar{N}(E)$ for the Richter data.

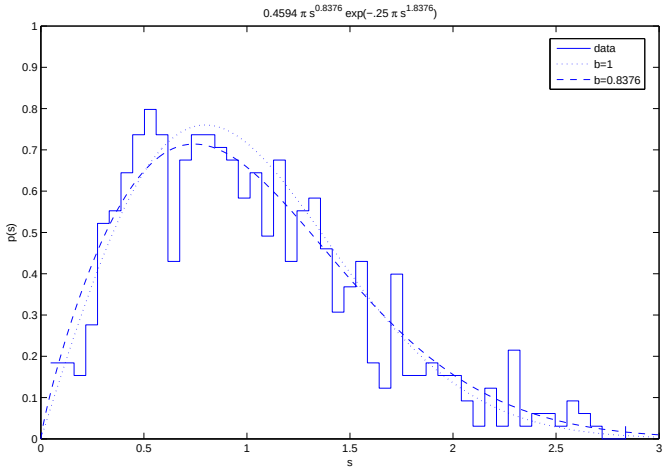

Figure 3.10: NNSD histogram real date, the best fitting Brody distribution and Wigner distribution

The Q-Q plot in Fig. 3.11 shows that distribution with cdf $F(S) = 1-\exp(-0.25\pi s^{1.8376})$ fits the unfolded eigenvalues of the real data.

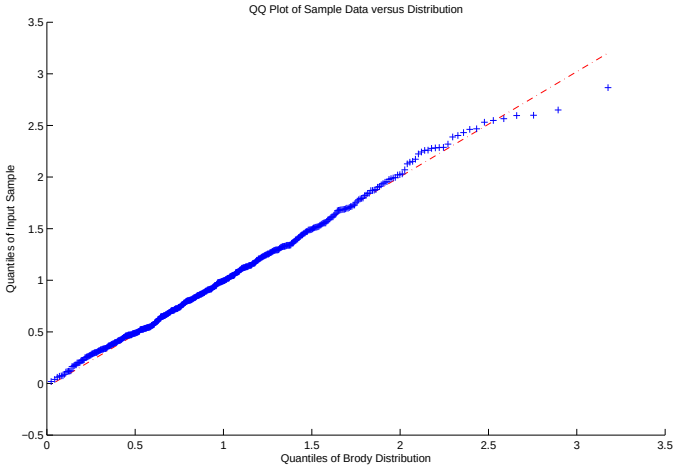

Figure 3.11: Quantiles of Wigner distribution vs. quantiles of unfolded real data.

Note that the repulsion parameters of the two distributions fitted to the unfolded eigenvalues corresponding to periodic kernel and the real data($b = 0.8755$ and $b = 0.8376$ respectively) are remarkably close to each other; in particular, one can expects that they are fitted to the same distribution. The Q-Q plot in Fig. 3.12 demonstrates that this is indeed very likely.

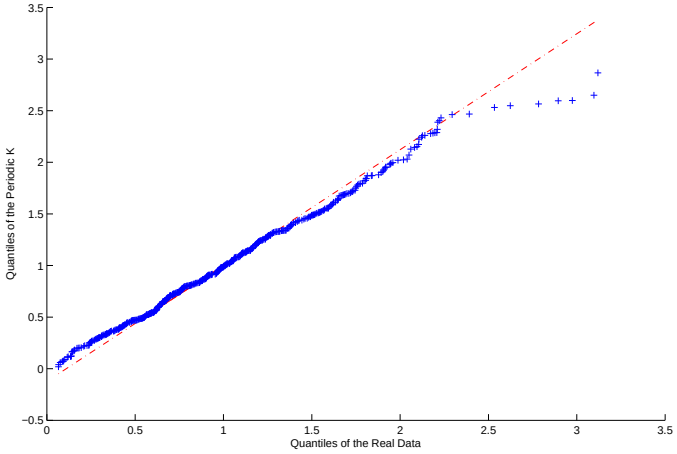

Figure 3.12: Quantiles of unfolded real data vs. quantiles of unfolded eigenvalues corresponding to the periodic K.

Applying the same methods to the data those presented in Section 3.3, as well as tak-

ing steps 1 and 2 described in there, one is able to unfold the data and find the repulsion parameter b

Data	Repulsion parameter(b)
Richter	$0.52 \leqslant b \leqslant 1$

Table 3.2: The repulsion parameter b for Richter data.

and since $a = \frac{1}{\pi}(\Gamma(\frac{2+b}{1+b}))^{(1+b)}$ one obtains $a \in \{0.24, 0.25, 0.26, 0.27, 0.28, 0.29, 0.30\}$.

Appendix A

Some statistical tools

Assume we have data from a population of interest, and the goal is to model the underlying cumulative density function (cdf) F(x). The composite goodness of fit problem in this situation is assessing the null hypothesis:

$$F(x;\theta) = F_0(x;\theta) \quad \text{for all x and some} \quad \theta \tag{A.0.1}$$

where $F_0(x;\theta)$ is a completely specified cdf.

Of particular interest are parametric location-scale families

$$F(x) = F_0(\frac{x-\mu}{\sigma}) \tag{A.0.2}$$

where μ is a location parameter and σ is a scale parameter.

In order to solve problem A.0.1 statisticians usually apply two different methods, graphical methods and goodness-of-fit tests. Both methods have their own advantages and disadvantages. Graphical methods allow one to visually examine the data and look for symmetric pattern and if the distribution does not fit the data they will suggest the alternative models. However, this approach is subjective. On the other hand, goodness-of-fit tests provide rigorous criteria for accepting and rejecting a hypothesis. However, if a hypothesis is rejected they give little inkling as to which alternative distribution may be appropriate. By combining the graphical methods and confidence band one can use the two methods for their respective advantages [27].

A.1 Quantile-Quantile plot (Q-Q plot)

Assume we are given a numerical sample $X_1, X_2, \cdots, X_n$ independent and identically distributed from $F(x)$ (iid~ $F(x)$), and we wish to know if $F(x)$ can be approximated by a given distribution $F_0(x)$. We can estimate $F(x)$ by the emperical distribution function

(ecdf):

$$\hat{F}(x) = \frac{1}{n}\sum_{i=1}^{n} H(X_i \leqslant x)$$

where

$$H(X_i \leqslant x) = \begin{cases} 1 & X_i \leqslant x, \\ 0 & \text{otherwise} \end{cases}$$

Let the values X_i be arranged in an increasing order $X_{(1)} \leqslant X_{(2)} \cdots \leqslant X_{(n)}$. Then, ecdf is a step function that jumps a height of $\frac{1}{n}$ at the value of each order statistic $X_{(i)}$. An effective way to check a distributional assumption is to construct the $Q-Q$ plot. If the distribution on which the plot is based is correct, the points in the plot stay close to a straight line. The Q-Q plot is a plot of the quantiles from the hypothesized cdf against the quantiles from the ecdf . More specifically, let $F_0^{-1}(p)$ be the pth quantile (=the 100pth percentile) of the hypothesized cdf. Then, the Q-Q plot is a plot of

$$F_0^{-1}(\frac{i-0.5}{n}) \quad \text{vs.} \quad X_{(i)}.$$

[27] The 100pth percentile is the number $\eta(p)$ that satisfies $F(\eta(p)) = p$. That is, $\eta(p)$ is the number on the measurement scale such that the area under the density curve to the left of $\eta(p)$ is p [20].

Equivalently the Q-Q plot is a plot of $F_0^{-1}(\hat{F}(x))$, i.e., a plot of the ecdf $\hat{F}(x)$ with the y-axis transformed [27]. If the location-scale model A.0.2 holds, it is easy to see that $F_0^{-1}(\hat{F}(x))$ is approximately equal to $\frac{x-\mu}{\sigma}$. Thus the Q-Q plot is linear with slope $\frac{1}{\sigma}$ and intercept $\frac{-\mu}{\sigma}$. This suggests that location-scale model is reasonable. So we can verify the location-scale hypothesis by checking if the Q-Q plot follows a line without considering its slope and interception. Thus, we can use the same Q-Q plot, without any modification, to check the fit of an entire location-scale family of cdfs.

So far we have assessed a non-parametric distribution. To extend the Q-Q plot method to a parametric families of distributions, first we have to estimate the unknown parameters. Two methods of maximum likelihood and moment estimate can be used to estimate these parameters.

- ***The Method of Moments [20].*** Let $X_1, \cdots, X_n$ be a random sample from a distribution $f(x)$. The kth population moment is $E(X^k)$ and kth sample moment is $\frac{1}{n}\sum_{i=1}^{n} X_i^k$.

  Now, let $X_1, \cdots, X_n$ be a random sample from a distribution $f(x; \theta_1, \cdots, \theta_m)$, where θ_i is a parameter whose value is unknown. Then the moment estimator $\bar{\theta_i}$ is obtained by equating the first m sample moments to the corresponding first m population moments which are functions of parameters and solve for θ_i.

- ***Maximum likelihood estimation [20].*** Let $X_1, \cdots, X_n$ jointly distributed by $f(x_1, \cdots, x_n; \theta)$ where θ has unknown value. The maximum likelihood estimate $\hat{\theta}$ is the value of θ that maximaizes f

$$f(x_1, \cdots, x_n; \hat{\theta}) \geqslant f(x_1, \cdots, x_n; \theta) \quad \text{for all } \theta$$

  One can extend maximum likelihood estimation to more than one parameter.

A.2 The Kolmogorov-Smirnov test

Since the interpretation of Q-Q plots might be different from person to person and can be difficult statisticians developed the idea of confidence bands that allow them to explain the uncertainty in the Q-Q plots and to provide more objective assessments. The most well-known confidence band for $F(x)$ is the Kolmogorov band (K-band):

$$(\hat{F}(x) - \frac{c_\alpha}{\sqrt{n}}, \hat{F}(x) + \frac{c_\alpha}{\sqrt{n}})$$

where c_α is the $100(1-\alpha)$th percentile of a corresponding test statistic. That is, the probability that the band will contain the true F(x) for all x is at least $(1-\alpha)$.
There is a one to one correspondence between the K-band and the Kolmogorov test statistic:

$$K = max|\hat{F}(x) - F_0(x)| \quad x \in \mathbb{R}$$

The Kolmogorov statistic has this property that, if the null hypothesis A.0.1 holds and if $F_0(x)$ is continuous and increasing, then it is distribution free. That is, it does not depend on what $F_0(x)$ is.

For convenience, we assume $\hat{F}(x) = F_n(x)$, where n is the total number of outcomes of sample, and

$$K_n = max|F_n(x) - F_0(x)| \quad x \in \mathbb{R}.$$

When the null hypothesis is true, the probability distribution of K_n is a distribution which is the same for any possible $F_0(x)$ and that does not depend on the particular $F_0(x)$ being studied in a specific problem. If the null hypothesis is true, then $\lim_{n\to\infty} K_n = 0$ which is the Glivenko-Cantelli theorem, see [19].

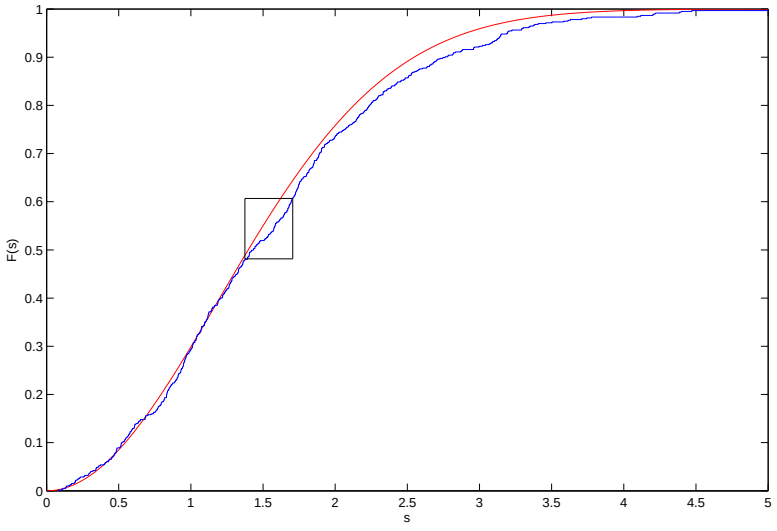

Figure A.1

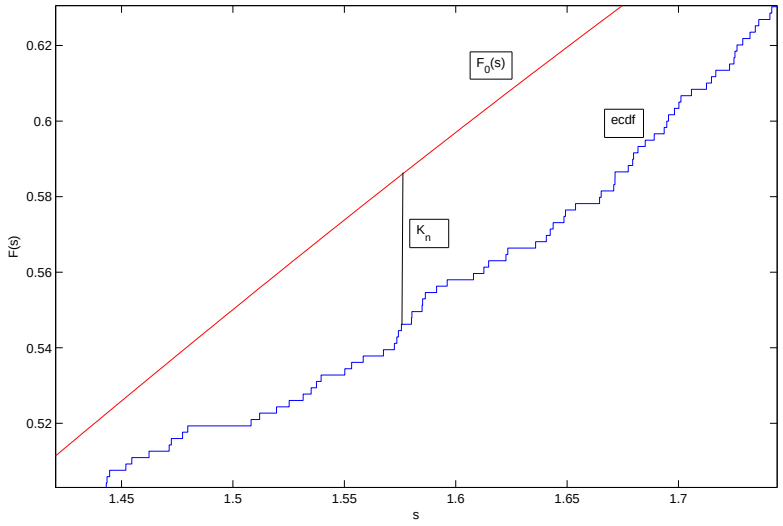

Figure A.2

If the null hypothesis is true, then for any given value $s > 0$,

$$\lim_{n\to\infty} p(\sqrt{n}K_n \leqslant s) = H(s) = 1 - 2\sum_{i=1}^{\infty}(-1)^{i-1}\exp(-2i^2s^2).$$

We can write approximate the right hand side of the above equation as

$$H(s) \simeq 1 - 2\exp(-2s^2)$$

[58]. A test procedure which reject the null hypothesis when $\sqrt{n}K_n > c_\alpha$ is called Kolmogorov-Smirnov test.

We can find c_α from the following equation

$$1 - \alpha = H(c_\alpha) \simeq 1 - 2\exp(-2c_\alpha^2)$$

then

$$c_\alpha \simeq \sqrt{\frac{-1}{2}\log(\frac{\alpha}{2})}.$$

Therefore, Kolmogorov-Smirnov test rejects the null hypothesis if

$$c_\alpha > \sqrt{\frac{-1}{2}\log(\frac{\alpha}{2})}.$$

Accordingly, The Kolmogorov confidence band is

$$(\hat{F}(x) - \sqrt{\frac{-1}{2n}\log(\frac{\alpha}{2})}, \hat{F}(x) + \sqrt{\frac{-1}{2n}\log(\frac{\alpha}{2})}).$$

Now, for example, if $\alpha = 0.05$, the confidence band is

$$(\hat{F}(x) - \frac{1.36}{\sqrt{n}}, \hat{F}(x) + \frac{1.36}{\sqrt{n}}),$$

where 1.36 is 95th percentile of kolmogorov test statistic K. That is, the probability that the band will contain the true $F(x)$ for all x is at least 0.95.

Appendix B
MATLAB Codes

B.0.1 The numerical algorithms corresponding to Chapter 2

In order to ensure reproducibility of the reported results we outline the numerical procedures. The main task is to construct the composite system Hamiltonians of type (2.2.1)-(2.2.3). Let X denote an $N \times N$ matrix representing the state of a composite system (—compare (2.2.2)). The preparatory phase consists of two parts: first, the construction of the interaction operator H_{int} which is a convolution type operator, roughly, $H_{int}[X] = K * X$ and second, the construction of a non-interacting composite system Hamiltonian of the form $\tilde{H} = H_1 \otimes I + I \otimes H_2$. Note that the operators act on matrices, and hence the main challenge is in representing these operators in a suitable basis in the space of matrices. We describe this in more detail below.

The input data consist of:

- A $p \times p$ matrix K (we take p odd for simplicity). Recall that for the final Hamiltonian to be a hermitian operator, $\check{K}$ must have real entries.
- Two N-vectors h_1 and h_2, each containing the ordered list of the eigenvalues of its corresponding subsystem Hamiltonian.
- A real number representing the coupling constant λ.

First, the interaction matrix H_{int} is built in steps as follows:

1. Choose a special basis in the space of $N \times N$ matrices as follows:

$$X_{11}, (X_{12}, X_{21}), (X_{13}, X_{22}, X_{31}), \cdots$$

(parentheses are only used to emphasize the pattern), where X_{ij} denotes a matrix with $X_{ij}(i, j) = 1$ and zeros elsewhere.

2. Define $C = conv2(K, X_{ij})$. Subsequently, select the $N \times N$ mid-centered sub-matrix of C and call it C_{ij}. (This is necessary because the numerical convolution algorithm results in an enlarged matrix which is inconsistent with the definition of H_{int}.)

3. Build an N^2-vector V_{ij} by reordering the entries of C_{ij} into a sequence, starting from the top right and proceeding through consecutive diagonals to the bottom left of C_{ij}. The following example illustrates the principle:

$$\text{If } C_{ij} = \begin{pmatrix} a_1 & a_2 & a_3 \\ b_1 & b_2 & b_3 \\ c_1 & c_2 & c_3 \end{pmatrix}, \text{ then } V_{ij} = [a_3, a_2, b_3, a_1, b_2, c_3, b_1, c_2, c_1]^T.$$

4. Build $N^2 \times N^2$ matrix H_{int} whose columns are vectors V_{ij} ordered in the same way as the X_{ij} in step 1.

Second, one constructs the non-interacting part of the Hamiltonian, i.e. $\tilde{H}$:

1. Define $H(i, j) = h_1(i) + h_2(j)$.

2. Build an N^2-vector W by reordering the entries of H in a way analogous to step 3 above.

3. Define: $\tilde{H} = \text{diag}(W)$ (a diagonal matrix with W filling the diagonal).

At this stage one is ready to define the total Hamiltonian: $Hamiltonian = \tilde{H} + \lambda H_{int}$. The Hamiltonian is now represented by a matrix, and one can rely on the MATLAB's standard 'eig' command to find its eigenvalues. Note that MATLAB utilizes the QR iteration algorithm to compute the eigenvalues of a matrix.

B.0

```
function [G1,EIG, Hamiltonian, F,NofE] =
                                        Gblock_solvable(K,h1,h2,npoints,lambda)
n=length(h1);
n=length(h2);
p=length(diag(K));
C=zeros(n+p-1);
D=zeros(n^2);

%%% D represents the interaction term in Hamiltonian %%%

count1=1;
count2=0;
count3=1;
V=zeros(n^2,1);
H1=zeros(n);
L=fliplr(K);

% Below X is a member of basis for space of n by n matrices %

for j=2:2*n
    for i=1+count2:j-1-count2
            X=zeros(n);
            X(i,j-i)=1;
            C=conv2(lambda*L,X);
          % C1=conv2(K,X,'same')
            C1=C((p-1)/2+1:n+(p-1)/2,(p-1)/2+1:n+(p-1)/2);

%%% C1 is the middle submatrix of C %%%
```

```
            F=fliplr(C1);
            m=length(diag(C1));
            count=1;
        for s=1:2*m-1
                T=diag(F,m-s);
            for t=1:length(T)
                V(count)=T(t);
                count=count+1;
            end
        end
                D(:,count1)=V;
                count1=count1+1;

    end
                if (j>n)
                    count2=count2+1;
                else
                    count2=0;
                end
end
D;

%%% D is the  interacction term %%%

for i=1:n
    for j=1:n
        H1(i,j)=h1(i)+h2(j);
    end
end
```

```
H2=fliplr(H1);
for s=1:2*n-1
    U=diag(H2,n-s);
    for t=1:length(U)
        W(count3)=U(t);
        count3=count3+1;
    end
end
H3=diag(W);
Hamiltonian = H3+D;
EIG = eig(H3+D);
 Peaks = lshift(NofE) - NofE;
 subplot(2,1,1);
 bar(E,Peaks); title('Eigenvalue peaks')

 subplot(2,1,2);



 plot(E,NofE,'k'); title('N(E)'); drawnow
 hold on
 plot([(n+1)/2,(n+1)/2],[0,NofE(npoints*(n+1)/2)])
 hold on
 plot([0,E(npoints*(n+1)/2)],[NofE(npoints*(n+1)/2),NofE(npoints*(n+1)/2)])
 hold on
end
```

Following code is conducted in order to create Figure 2.7:

```
function [KAP] = kapa(K,h1,h2,npoints,v,T,Ef)
```

```
n=length(h1);
n=length(h2);
p=length(diag(K));
C=zeros(n+p-1);
D=zeros(n^2);
kapa=zeros(1,T);
lambda=[1:T];
%%% D represents the interaction term in Hamiltonian %%%
for u=1:T
count1=1;
count2=0;
count3=1;
count4=0;
V=zeros(n^2,1);
H1=zeros(n);
L=fliplr(K);

%%% in following X is a member of basis for space of n by n matrices
%%%
for j=2:2*n
    for i=1+count2:j-1-count2
            X=zeros(n);
            X(i,j-i)=1;
            C=conv2(u*L,X);
           % C1=conv2(K,X,'same')
             C1=C((p-1)/2+1:n+(p-1)/2,(p-1)/2+1:n+(p-1)/2);
             F=fliplr(C1);
            m=length(diag(C1));
            count=1;
```

```
        for s=1:2*m-1
            T=diag(F,m-s);
            for t=1:length(T)
            V(count)=T(t);
            count=count+1;
            end
        end
            D(:,count1)=V;
            count1=count1+1;

    end
              if (j>n)
                  count2=count2+1;
              else
                  count2=0;
              end
end
D;
for i=1:n
    for j=1:n
        H1(i,j)=h1(i)+h2(j);
    end
end
H2=fliplr(H1);
for s=1:2*n-1
    U=diag(H2,n-s);
    for t=1:length(U)
        W(count3)=U(t);
        count3=count3+1;
```

```
    end
end
H3=diag(W);
Hamiltonian = H3+D;
EIG = eig(H3+D);

F=unique(EIG);
F1=F(1:(n*(n+1)/2))
F1=real(F1);
total = length(F1);
E = linspace(0,ceil(max(F1)),npoints*ceil(max(F1)));
NofE = zeros(size(E));

for l = 1:total  %parfor
    NofE = NofE + (E>F1(l));
end

kapa(u)=NofE(v)-(n+1)/2;
kapa;
plot(lambda,kapa,'k')
hold on
end
```

B.0.2 The numerical algorithms corresponding to Chapter 3

In order to ensure reproducibility of the reported results we outline the numerical procedures. The main task is first to find the unfolded spectrum results from the Hamiltonian (2.2.1)-(2.2.3) and then fit the unfolded spectrum to the Brody type (3.2.4) distribution for appropriate repulsion parameter. The numerical algorithm consists of two parts. Part

one comprises a function which accepts the eigenvalues of the Hamiltonian as an input and gives unfolded eigenvalues as an output. Part two consists of another function which accepts the unfolded eigenvalues results from part one and gives the repulsion parameter (b). Thus the Brody distribution is fitted to the unfolded eigenvalues.

1. Part one

   The input data consists of:

   - A vectore K consists of eigenvalues of the Hamiltonian.
   - Two real numbers c and d determining an interval on energy axis.
   - A real number t to divide interval $[c, d]$ to subintervals.

   Interpolating $N(E)$ by $\bar{N}(E)$:

   - Evaluate difference of any two adjacent eigenvalues in each subinterval.
   - Find an appropriate polynomial to be fitted to the eigenvalues of the Hamiltonian and take a derivative of that and evaluate the derivative at the middle point of each subinterval.
   - Multiply the results of two previous steps in each individual subinterval.

   Output:

   - We obtain a sub-vector for each subinterval. Coalescing the sub-vectors yields a vector S which contains of all unfolded eigenvalues of the Hamiltonian.

2. Part two

   The input data consists of:

   - Vector S, unfolded eigenvalues.

   Fitting data to a Brody type distribution:
   Fit vector S to the CDF (cumulative density function)

$$F(S) = 1 - \exp(-a\pi S^b)$$

for appropriate parameter a and b resulting from next step.

- Obtain vector F for different $a, b \in [0.1, 2]$.
- Obtain vector G=[S F].
- Utilize the "kstest", a built-in function of MATLAB, H=kstest(S,G,.05). If H==0, print a and b.

Remark 1. *The returned value of $H = 1$ indicates that kstest rejects the null hypothesis (Brody distribution) at the default 5 percent significance level. It means we are about 95 percent confident that we have made the right decision. In other words, we could be wrong with probability 0.05.*

```
%s is unfolded eigenvalues
index=0;

for a=10:1:200
    for b=10:1:200
        F=1-exp(-(a/100)*pi*s.^(b/100));%(periodic K and Richter)

        G=[s F];
        [H,p]=kstest(s,G,.05);
 %(kstest is a standard MATLAB function to perform Kolmogorov-Smirnov test)
      if H==0
        index=index+1;
        c=[a b];
        disp(c)
        disp(a)
        disp(b)
      end
   end
```

```
end

%%%%%%%%%%%%%%%%%%%%%%%%%%%%%%%%%%%%%%%%%%%%%%%%%%%%%%%%%%%%%%%%%%%%%%%%%%%%%%%%
 for a=1:1:100


        F=1-exp(-(a*pi/100)*s); %(Special K)
        G=[s F];
        [H,p]=kstest(s,G,.05);
       if H==0
          index=index+1;
          disp(a)
        % B(index)=a;
        %P(index)=p;
       end


 end



%%%%%%%%%%%%%%%%%%%%%%%%%%%%%%%%%%%%%%%%%%%%%%%%%%%%%%%%%%%%%%%%%%%%%%%%%%%%%%%%
 for a=1:1:100
     %F=1-exp(-(1-(a/100))*s-(a/100)*(.7+.3*(a/100))*((pi*s.^2)/4));
     F=1-exp(-(a/100)*s-(pi/4)*(1-a/100)*s.^2);
        G=[s F];
       [H,p]=kstest(s,G,.05);
       if H==0
        disp(a)
       end
 end
end
```

```
function [F_clean,p] = unfold(K,a,b,t )

 E=K(K>=a & K<=b);
  A=[a:t:b];
for i=1:length(A)-1

 F= E(E>= A(i) & E<A(i+1));
G=(lshift(F)-F)* (7*(A(i+1)+A(i))/2-1.3)
%multiply by derivative of the polynomial which fit the N(E) curve.(Richter)
G=(lshift(F)-F)*
                (7.0416*(A(i+1)+A(i))/2-1.3037-1);
G=(lshift(F)-F)*
                (-.057*((A(i+1)+A(i))/2)^2+8*(A(i+1)+A(i))/2-4.9);(Richter)
G=(lshift(F)-F)*
                (-0.0114*((A(i+1)+A(i))/2)^2+1.4576*((A(i+1)+A(i))/2)-3.5614);
                                                                (periodic K)
G=(lshift(F)-F)*
                (-0.0067*((A(i+1)+A(i))/2)^2+1.2630*((A(i+1)+A(i))/2)-2.1081);
                                                                 (special K)
M(i,1:length(G))=G;
end
 M;
 N=M(:);
 p=N(N>0)

%% hist(p,25)
%% h = findobj(gca,'Type','Patch');
%% set(h,'FaceColor',[1 1 1], 'EdgeColor','black');
    [counts,bins]=hist(p,50);
```

```
%counts1=(50/3.5)*(1/sum(counts)).*counts %(periodic K)(50/6 old one)
 counts1=(50/4)*(1/sum(counts)).*counts %(Special K)(50/8 old one)
%counts1=(50/3)*(1/sum(counts)).*counts; %(Richter )
stairs(real(bins),counts1)
```

Following code create Figure 3.9 and its fitting curve.

```
function []= Richter_NofE(Richter)
npoints=100000;
 E = linspace(0,ceil(max(Richter)),npoints*ceil(max(Richter)));
% E = linspace(0,ceil(max(Richter)),ceil(max(Richter)));%new
NofE = zeros(size(E));
for l = 1:length(Richter) %parfor

        NofE = NofE + (E>Richter(l));
end

 Peaks = lshift(NofE) - NofE;
 subplot(2,1,1);
 bar(E,Peaks); title('Eigenvalue peaks')
 subplot(2,1,2);
 plot(E,NofE,'k'); title('N(E)'); drawnow % ORIGINAL
 plot(E*4/45,(1/(max(NofE)))*(NofE),'k'); title('N(E)'); %new

 hold on
 p=polyfit(E,NofE,3)
 pprime=polyder(p)
 y=polyval(p,E);
 %plot(E,NofE,'0',E,y)
```

```
 plot(E,y,'linestyle','--','color','g')
 axis([0 20 0 600])
end
```

Although MATLAB has a built-in function to draw Q-Q plots, following code is conducted in order to create Q-Q plots as well.

```
function[]=q_plot(S,a,b)

% For speccial K assume b=1 %

syms s
 F(s)=finverse(1-exp(-(a/100)*pi*s.^(b/100)),s) %(periodic K and Richter)
%F(s)=finverse(1-exp(-(a/100)*s.^b),s) %(Special K)
 T=sort(S);
n=length(S)

A=((1-.5)/n):1/n:((n-.5)/n);
G=F(A);

length(A);
G=eval(G);
length(G);
scatter(G,T)
%qqplot(G,T)
end
```

References

[1] Ashraf A. Abul-Magd and Adel Y. Abul-Magd. Unfolding of the spectrum of chaotic and mixed systems. *Physica A*, 396:185–194, 2004.

[2] R. C. Ashoori. Electrons in artificial atoms. *Nature*, 379:413, February1996.

[3] R. Ballian and C. Bloch. Distribution of eigenfrequencies for the wave equation in finite domain i. *Ann. Phys.*, 60:401, 1970.

[4] R. Ballian and C. Bloch. Distribution of eigenfrequencies for the wave equation in finite domain ii. *Ann. Phys.*, 64:271, 1971.

[5] R. Ballian and C. Bloch. Distribution of eigenfrequencies for the wave equation in finite domain iii. *Ann. Phys.*, 69:76, 1972.

[6] M. V. Berry. Semiclassical theory of spectral rigidity. *Proc. R. Soc. London Ser. A*, 400:229–251, 1985.

[7] M. V. Berry and M. Tabor. Level clustering in the regular spectrum. *Proc. Roy. Soc. (London) A*, 356:375, 1977.

[8] R. Blümel. *Advanced Quantum Mechanics*. Jones And Bartlett Publishers, Sudbury, Massachusetts, 2011.

[9] O. Bohigas, M. J. Giannoni, and C. Schmit. Characterization of chaotic quantum spectra and universality of level fluctuation laws. *Phys. Rev. Lett.*, 52(1):1–4, 1984.

[10] B. Booss and D.D. Bleecker. *Topology and Analysis*. Springer, New York, 1985.

[11] A. Bottcher and S.M. Grudsky. *Spectral Properties of Banded Toeplitz Matrices*. SIAM, 2005.

[12] T. A. Brody. A statistical measure for the repulsion of energy levels. *Letter Al Nuovo Cimento*, 7(12):482–484, 1973.

[13] T. A. Brody, J. Flores, J. B. French, P. A. Mello, A. Pandey, and S. S. M. Wong. Random-matrix physics: spectrum and strength fluctuations. *Reviews of Modern Physics*, 53(3):385, 1981.

[14] H. Bruus and K. F. Fleensberg. *Many-body quantum theory in condensed matter physics.* OUP, New York, 2006.

[15] H. Buch, S. Mahapatara, R. Rahman, A. Morello, and M. Y. Simmons. Spin readout and addressability of phosphorus-donor cluster in silicon. *Nature communications*, 2013.

[16] S. Datta. Nanoscale device modeling: the Green's function method. *Superlattices and Microstructures*, 28(4), 2000.

[17] S. Datta. The non-equilibrium green's function (negf) formalism: an elementary introduction. *IEEE*, page 703, 2002.

[18] S. Datta. *Lessons from Nanoelectronics.* World Scientific, Singapore, 2012.

[19] M. H. DeGroot. *Probability and statistics.* Addison-Wesley, 1986.

[20] J. L. Devore. *Probability and statistics for engineering and sciences.* Wadsworth, Inc, 1995.

[21] D. P. Divencenzo. Double quantum dot as a quantum bit. *Science*, 309:2173, 2005.

[22] F. J. Dyson. Statistical theory of the energy levels of complex systems i. *Journal of Mathematical Physics*, 3(1):140–156, 1962.

[23] F. J. Dyson. Statistical theory of the energy levels of complex systems ii. *Journal of Mathematical Physics*, 3(1):157–165, 1962.

[24] F. J. Dyson. Statistical theory of the energy levels of complex systems iii. *Journal of Mathematical Physics*, 3(1):166–175, 1962.

[25] B. Eckhardt. Quantum mechanics of classically non-integrable systems. *Physics Reports*, 163(4):205–297, 1988.

[26] L. D. Faddeev and O. A. Yakobovskii. *Lectures on quantum mechanics for mathematical students.* AMS, Providence, Rohde Island, 2009.

[27] A. E. Freeny and V. N. Nair. Methods for assessing distributional assumption in one- and two-sample problems. In J. L. Stanford and S. B. Vardeman, editors, *Statistical methods for physical scince.* Academic Press, 1994.

[28] A. Friedman. *Foundations of modern analysis*. Holt, Rinehart and Winston, Inc., 1970.

[29] T. Fujisawaa, .T Hayashi, H.D. Cheongb, Y.H. Jeongc, and Y. Hirayamaa;d. Rotation and phase-shift operations for a charge qubit in a double quantum dot. *Physica E*, 21:1046–1052, 2004.

[30] C. W. Gardiner and P. Zoller. *Quantum noise*. Springer, Berlin, 2000.

[31] H. D. Gräf, H. L. Harney, H. Lengeler, C. H. Lewenkopf, C. Rangacharyulu, and A. Richter. Distribution of eigenmodes in a superconducting stadium billiard with chaotic dynamics. *Phys. Rev. Lett.*, 69(9):1296, 1992.

[32] T. Guhr, A. Müller-Groeling, and H. A. Weidmüller. Random matrix theory in quantum physics: common concepts. *Physics Reports*, 299(4-6):1–178, 1998.

[33] S. J. Gustafson and I. M. Sigal. *Mathematical concepts of quantum mechanics*. Springer-Verlag, Berlin Heidelberg, 2011.

[34] M. C. Gutzwiller. Phase integral approximation in the momentum space and the bound states of an atom i. *J. Math. Phys.*, 8(10):1979, 1967.

[35] M. C. Gutzwiller. Phase integral approximation in the momentum space and the bound states of an atom ii. *J. Math. Phys.*, 10(6):1004, 1969.

[36] M. C. Gutzwiller. Classical quantization of a hamiltonian with ergodic behavior. *Phys. Rev. Lett*, 45:150, 1980.

[37] M. C. Gutzwiller. *Chaos in classical and quantum mechanics*. Springer, New York, 1990.

[38] B. C. Hall. *Quantum theory for mathematicians*. Springer, New York, 2013.

[39] U. Harbola, M. Esposito, and S. Mukamel. Quantum master equation for electron transport through quantum dots and single molecules. *Phys. Rev B*, 74:235309, 2006.

[40] E.T. Jaynes and F.W. Cummings. Comparison of quantum and semiclassical radiation theories with applications to the beam maser. *Proc. IEEE*, 59(89), 1963.

[41] T. Junno, S. B. Carlsson, H. Q. Xu, L. Samuelson, and A. O. Orlov. Single-electron tunneling effects in a metallic double dot device. *Applied Physics Letter*, 80(4):667–669, 2002.

[42] M. Kac. Can one hear the shape of a drum? *Amer. Math. Monthly.*, 73(4):1–23, 1966.

[43] J. Keating. The quantum mechanics of chaotic systems or can one hear the chaology of a drum? In T. Mullin, editor, *The Nature of Chaos*. OUP, 1993.

[44] L. V. Keldysh. Diagram technique for non-equilibrium processes. *Sov. Phys. JETP*, 20:1018, 1965.

[45] K. Klantar-Zadeh and B. Fry. *Nanotechnology-Enabled Sensors*. Springer, New York, USA, 2008.

[46] L. P. Kouwenhoven, D. G. Austing, and S. Tarucha. Few-electron quantum dots. *Rep. Prog. Phys.*, 64:701–736, 2001.

[47] J.B Lawrie and I.D. Abrahams. A brief historical perspective of the Wiener-Hopf technique. *Engrg. Math*, 59(4):351–358, 2007.

[48] T. J. Levy and E. Rabani. steady state conductance in a double quantum dot array: The nonequilibrium equation of motion green's function approach. *The Journal of Chemical Physics*, 138:164125, 2013.

[49] Xin-Qi Li, JunYan Luo, and Yong-Gang Yang. Quantum master-equation approach to quantum transport through mesoscopic systems. *Physical Review B*, 71:255304, 2005.

[50] K. Likharev. Single -electron devices and their applications. *IEEE*, 87(4):606–632, 1999.

[51] K. Likharev and T. Cleason. Single electronics. *Scientific American*, June 1992.

[52] E. Lipparini. *Modern many-particle physics*. World Scientific, Singapore, 2003.

[53] J-L. Liu. Mathematical modeling of semiconductor quantum dots based on the non-parabolic effective-mass approximation. *Nanoscale Systems MMTA*, 1(1):58, 2012.

[54] P. C. Martin and J. Schwinger. Theory of many particle systems i. *Phys. Rev.*, 115:1342, 1959.

[55] S. W. McDonald and K. N. Kaufman. Wave chaos in the stadium: statistical properties of short-wave solutions of the helmholtz equation. *Phys. Rev. A*, 37:3067, 1988.

[56] M. Mehta. *Random Matrices*. Academic Press, San Diego, 2004.

[57] E. Ott. *Chaos in dynamical systems*. Cambridge University Press, 1993.

[58] A. Papoulis and A. U. Pillai. *Probability, random variables and stochastic processes*. McGraw-Hill, 2002.

[59] M. Paulsson, F. Zahid, and S. Datta. Electrical conduction through molecules. *Advanced Semiconductors and Organic Nano-Techniques*, 2003.

[60] J. N. Pedersen and A. Wacker. Tunneling through nanosystems: Combining broadening with many-particle states. *Physical Review B*, 72:195330, 2005.

[61] J. R. Petta, A. C. Johnson, J. M. Taylor, E. A. Laird, A. Yacoby, and M. D. Lukin et al. Coherent manipolation of coupled electron spin in semiconductor quantum dots. *Science*, 309:2180, 2005.

[62] C. E. Porter. *Statistical Theories of Spectra: Fluctuations*. Academic Press, New York, 1965.

[63] A. Rastelli, S. Kiravittaya, and O. Schmidt. Growth and control of optically active quantum dots. In P. Michler, editor, *Single Semiconductor Quantum Dots*. Springer-Verlag, 2009.

[64] M. Reed and B. Simon. *Functional Analysis*. Academic Press, 1980.

[65] M. A. Reed. Quantum dots. *Scientific American*, page 118, January 1993.

[66] M. A. Reed, J. N. Randall, R. J. Aggarwall, R. J. Matyi, T. M. Moore, and A. E. Wetsel. Observation of discrete electronic states in a zero-dimensional semiconductor nanostructure. *Phys. Rev. lett.*, 60(6):535, 1987.

[67] A. Rybkin. Mathematical physics lecture notes, 2013.

[68] A. Shamloo and A. Sowa. A numerically efficient approach to the modelling of double-qdot channels. *Nanoscale Systems MMTA*, 2:145–156, 2013.

[69] G. Shinkai, T. Hayashi, T. Ota, and T. Fujisawa. Correlatd coherent oscillation in couple semiconductor charge qubit. *Superlattices and Micristructures*, 28(4), 2000.

[70] B. W. Shore and P. L. Knight. The Jaynes-Cummings model. *J. Mod. Opt.*, 40:1195, 1993.

[71] V. P. Singh, A. Agrawal, and S. B. Singh. Analytical discussion of single electron transistor (ser). *Inernational Journal of Soft Computing and Engineering (IJSCE)*, 2(3):502, 2012.

[72] S. Stenholm and K-A. Suominen. *Quantum approach to informatics*. John Wiley, 2005.

[73] D.M Sullivan. *Quantum mechanics for electrical engineers*. IEEE PRESS, 2012.

[74] D. Sztenkiel and R.Świrkowicz. Electron transport through quantum dot system with inter-dot coulomb interaction. *Acta Physica Polonica A*, 111(3):361–372, 2007.

[75] G. Teschl. *Mathematical methods in quantum mechanics: with application to Schrodinger operators*. AMS, 2009.

[76] L. N. Trefethen and M. Embree. *Spectra and Pseudospectra*. Princeton Univrsity Press, Princeton, New Jersey, 2005.

[77] R. Turton. *The physics of solids*. Oxford University Press, Oxford, 2000.

[78] S. E. Ulloa and D. Pfannkuche. Level statics and interactions in a two-dimensional quantum dot. *Superlattices and Microstructures*, 21(1):21–28, 1997.

[79] E. Wigner. On the statistical distribution of the widths and spacings of nuclear resonance levels. *Proc. Cambridge Phil. Soc.*, 47:790–798, 1951.

[80] E. Wigner. Statistical properties of real symmetric matrices with many dimensions. *Can. Math. Congr. Proc.*, page 174, 1957.

[81] A.M. Zagoskin. *Quantum Engineering*. Cambridge University Press, 2011.